Cranfield University

School of Engineering

MSc. Research Thesis

Academic Year: 2010 ~ 2011

QINGLIN MA

Aircraft Icing and Thermo-Mechanical Expulsion De-icing Technology

Supervisor: Dr. Craig Lawson

December 2010

ACKNOWLEDGEMENTS

I would firstly like to expresses special thanks to my family and friends for their continual support and encouragement, especially to my wife Mrs. Xiaolou Jing, whose patient love enabled me to complete the work.

I would like to extend my appreciation to Dr. Craig Lawson for his continuous support and kind help during the research project.

I would also like to thank Chinese Government and Aviation Industry Corporation for their supports and give me an opportunity to conduct MSc study in Cranfield University.

ABSTRACT

The topic of this thesis is Aircraft Icing and Aircraft Icing and Thermo-Mechanical Expulsion De-icing Technology. The main objectives are to investigate aircraft icing meteorology and effects on aircraft, ice protection systems and thermo-mechanical expulsion de-icing technology.

Initially, the research project focuses on aircraft icing meteorology, ice accumulation and icing effects on flight safety. A basic understanding of aircraft icing is explained, including icing conditions and parameters, ice detection, ice accretion shapes, and icing effects in terms of different airframe surfaces.

Ice protection systems are employed to prevent the icing hazards and ensure flight safety. The conventional and novel ice protection technologies are investigated and their characteristics are explained. Thermo-mechanical expulsion de-icing technology is selected as the research topic because of its typical characteristics of lower power required and high de-icing efficiency.

Methods are explored to assess power consumption of thermo-mechanical expulsion de-icing system. In addition, a thermo-mechanical expulsion de-icing system architecture is explored for a civil aircraft and system power consumption is calculated. In order to explain the system design characteristics, conventional electro-thermal de-icing system architecture is designed to show the contrasts in terms of power consumption, de-icing efficiency, cost and mass.

This novel ice protection system has better results in power consumption and de-icing performance, allowing long time flight in icing conditions. It can compensate the disadvantages of heavier mass and higher cost because there is no need to escape from icing encounters immediately and fuel penalties are reduced sequentially.

CONTENTS

LIST OF FIGURES

LIST OF TABLES

LIST OF ABBREVIATIONS

AFIDS	Advisory Flight Icing Detection System
DCU	De-icing Control Unit
EIDS	Electro-Impulse De-icing System
EMEDS	Electro-Magnetic Expulsion De-icing System
ESB	Energy Storage Bank
ETDS	Electro-Thermal De-icing System
IDS	Icing Detection System
IPS	Ice Protection System
LWC	Liquid Water Content
MOAS	Method of Assumed States
MVD	Medium Volume Diameter
OAT	Outside Air Temperature
PCU	Power Control Unit
PETDS	Pulse Electro-Thermal De-icing System
PFIDS	Primary Flight Icing Detection System
SLD	Supercooled Large Drops
TMEDS	Thermo-Mechanical Expulsion De-icing System
WHC	Wing Heat Controller

NOTATION

Symbols

b	Width, m
c	Specific Heat Capacity, J/(kg℃)
C	Heat Capacity, J/℃; Capacitance, Fa; Chord Length, m
d	Thickness/Distance, m
D	Diameter, m
E_m	Water Catch Efficiency
F	Electromagnetic Force, Newton
h_c	Convective Coefficient, W/（m^2℃）
I , i	Electrical Current, Ampere
l	Length, m
L	Inductance, H
m	Mass, kg
N	Number
P	Electrical Power Consumption, W; Pressure, Pa
q	Anti-icing Heat Load, W
Q	Energy Consumption, J
R	Resistance
t	Time, s
T	Temperature, ℃
V	Velocity, m/s
α	Coefficient of Heat Diffusivity, m^2/s
β	Local Water Catch Efficiency
γ	Latent Heat of Fusion, J/kg
λ	Thermal Conductivity Coefficient, W/（m℃）
ρ	Density, kg/m^3

Superscripts

n	Time Interval

Subscripts

0	Ambient and Initial
a	Air
c	Convective
e	Evaporation
EXT	Exterior Surface
h	Heater
i	Ice, Spatial Increment
I	Interface
INT	Interior Surface
j	Different Shedding Layers
ke	Kinetic Energy
L	Liquid Phase
m	Melted
p	Constant Pressure
s	Substrate of Airfoil, Surface
S	Solid Phase
sat	Saturated
v	Viscosity
w	Water

1 Introduction

1.1 Background

In-flight icing has seriously hazardous effects on aircraft safety. Ice builds on the leading surfaces of the aircraft, not only on the wings, empennages, propellers, and windshields, but also on the antennas, vents, intakes, and nacelle lips. The accumulation of ice on the wings and empennages destroys the smooth air flow, resulting in lift decrease, drag increase, degraded maneuverability and stability. The aircraft may stall at much higher speeds and lower angles of attack than normal. Propeller icing may cause propulsion loss. Antennas may vibrate severely and even break down because of icing. It must be mentioned that the icing on the engine nacelle lips may cause air flow turbulence in the inlet and result in engine vibration, propulsion loss, and even surging. Besides that, ice bulk ingestion may damage engine structure and cause much more serious problems.

Ice Protection System (IPS) is employed to ensure aircraft flight safety during icing conditions. Up to now, various types of IPS have been developed, such as hot-air anti-icing system, electro-thermal de-icing system, pneumatic boot de-icing system, electro-impulse de-icing system and so on. IPS requires high performance efficiency and low power consumption in modern aircraft. However, no single ice protection type can meet these requirements, thus a hybrid ice protection technology is developed to solve this problem, named Thermo-Mechanical Expulsion De-icing System (TMEDS). TMEDS combines Pulse Electro-Thermal De-icing System (PETDS) and Electro-Magnetic Expulsion De-icing System (EMEDS) together [1]. More details about different ice protection systems will be discussed in Chapter 4.

1.2 Research Objectives

This research consists of three main parts. The first one is an investigation into the aircraft icing atmosphere and effects on aerodynamics. The objectives of this research

are listed below:

a) Investigate aircraft icing meteorological conditions and find out aircraft icing characteristics exposed in different types of clouds.
b) Research icing meteorological parameters and discuss the effects of meteorological parameters on aircraft ice accumulation and ice protection system. In addition, design specifications will be introduced briefly.
c) Analyze icing effects on aircraft different parts, including lift surfaces, engine and nacelle, windshield and sensors.

The second part is concerned with various ice protection systems. The research topics include:

a) A preliminary study different ice protection technology, outline the technical advantages and limitations and give some design concerns.
b) A brief look at some examples of the typical applications of IPS.
c) A more in depth investigation into the hybrid ice protection system (TMEDS) and a definition of the system characteristics.

The third part of the project involves power consumption calculations and analysis for TMEDS. The following points show the research scope for this category.

a) Find out power consumption calculation methods for TMEDS and analyze the influence of system parameters on system de-icing power.
b) Research a TMEDS system architecture and calculate the power consumption.
c) Compare TMEDS with Electro-Thermal De-icing System (ETDS) in terms of power consumption, de-icing performance, mass and cost, and give conclusions.

1.3 Research Methodology

The methodologies used for this research are as follows:

a) For the first and second parts, survey the relative literature and summarize the key points.
b) Calculation methods for the third part are created through literature survey. The influences on performance by system parameters are illustrated by tables or figures.
c) Based on a civil aircraft, investigate the predominance and disadvantages of TMEDS through being compared with conventional electro-thermal de-icing system.

2 Icing Meteorology

Flight in icing condition causes ice accumulation on aircraft component surfaces. In the icing condition, supercooled water droplets are contained in clouds, which still remain in liquid state despite of being below freezing point. The amount and shape of ice depends on configuration of surface, flight speed, air temperature, water droplet diameter, liquid water content and exposure time in clouds. In this Chapter, cloud types, meteorological parameters, meteorology design conditions and icing detection technology are discussed.

2.1 Icing Cloud Types

There are two types of clouds in which ice forms on the aircraft surfaces: stratiform clouds and cumuliform clouds [2].

2.1.1 Stratiform Clouds

Stratiform clouds are horizontal layers, sometimes extending to hundreds of kilometers. Despite of long distribution in horizontal level, the thickness is relatively minor, usually up to 2 kilometers. The stratiform clouds are composed of three levels: high, middle and low [3].

The high level stratiform clouds are above 20,000 feet and comprised of ice crystals. The ice crystals have no contribution to airframe icing, such as the wing, empennage and windshield. However, the effects on engine and total pressure sensor should be considered.

The middle level stratiform clouds are from 6500 to 20,000 feet. This type is significant to aircraft icing, because of the solid and liquid water content. These stratiform clouds cover a large extent of area for thousands of miles, resulting in a long time exposure in icing environment. So the ice formation is relatively large and

causes more adverse effects on aircraft performance.

The low level stratiform clouds are normally below 6500 feet. During this altitude the icing is extremely important not only because of wide coverage but also high Liquid Water Content (LWC). However, supercooled water droplets do not exist in the low level stratiform in summer clouds because of the lower altitude. The temperature is above freezing point and aircraft icing is not common during a hot day. But on a cold day, especially in winter, aircraft icing should be given more attention.

There are various types of stratiform clouds in the air. Some typical examples are shown here. They are stratus, altostratus and cirrostratus [4], see Figure 2-1.

(a) Stratus Clouds

(b) Altostratus Cloud

(c) Cirrostratus Cloud

Figure 2-1 Typical View of Stratiform clouds

Stratus clouds belong to the low level clouds. These clouds look gray in color and distribute uniformly, covering most even all of the sky. The photograph of stratus clouds is shown in Figure 2-1(a).

Altostratus clouds are the middle high stratiform clouds, comprised of ice crystals and water droplets. The altostratus cloud usually looks gray or blue-gray in appearance, covering the whole sky. The light of sun or moon may travel through altostratus cloud. A typical view of altostratus cloud is illustrated in Figure 2-1(b).

Cirrostratus cloud has a wide distribution and appears at high altitude, which is a type of high level stratiform cloud. Ice crystals are the main composition of cirrostratus cloud. This cloud is very thin, white with a transparent look, and an example is given in Figure 2-1(c).

2.1.2 Cumuliform Clouds

Cumuliform clouds cover less area horizontally than stratiform clouds. However, the LWC is significantly higher, causing high ice accumulation on aircraft surfaces. Normally, the cumuliform clouds are classified into cumulus and cumulonimbus [2], see Figure 2-2.

Cumulus cloud is comprised of water droplets, appearing in puffy white or light gray clouds. It has the appearance of floating cotton balls. The outlines of cumulus clouds are relatively sharp and the base is flat. Generally, the cumulus clouds have a base altitude of 1,000 m and a width of 1,000 m. This cloud type has a vertical development and clearly edges and appears alone, in lines, or in clusters. A typical example is shown in Figure 2-2 (a).

(a) Cumulus Cloud

(b) Cumulonimbus Cloud

Figure 2-2 Typical View of Cumuliform clouds

The composition of cumulonimbus clouds is a mixture of ice crystals and water droplets. They are white, dense, thick and huge, generally known as thunderstorm clouds. A photograph of cumulonimbus cloud is shown in Figure 2-5 (b). The base of cumulonimbus cloud is usually from 400 to 1,000m, and can grow up to 10,000 m high. Cumulonimbus clouds are associated with heavy rain, hail, lightning and tornadoes.

The characteristics of stratiform clouds and cumuliform clouds are shown in Table 2-1.

Table 2-1 Characteristics of Stratiform Clouds and Cumuliform Clouds

Issues	**Stratiform Clouds**	**Cumuliform Clouds**
Distribution	Horizontal	Vertical
Area	Cover larger area	Cover smaller area
Liquid Water Content	Lower	Higher
Icing Intensity	Lighter	Heavier

2.2 Aircraft Icing Meteorological Parameters

The amount, shape and rate of icing mainly depend on meteorological and flight conditions. In this chapter, the meteorological parameters are discussed, which are temperature, liquid water content, droplet diameter, and cloud extent. These discussions focus on the meteorological parameter's effects on icing shapes and ice protection systems.

2.2.1 Temperature

Temperature of cloud is the most significant meteorology parameter. This parameter directly determines whether ice will form on the aircraft surface. The possibility of icing only occurs while the local air temperature is below freezing point. Furthermore, temperature determines the ice shape and structure. When temperature is near the freezing points, only a small fraction of the impinged water droplets will freeze on the surface, while the residual will freeze on the downstream surface. This presents the possibility of forming double-horns ice shapes.

It is also observed that a rime ice accumulates at colder temperatures while at higher temperatures a glaze ice accretes. Reference [5] lists the ice accretion characteristics of different icing conditions. Below, some results are extracted to explain the

temperature effects on icing accretion. The icing conditions are listed in Table 2-2[5] and the research results are shown in Figure 2-3[5].

Table 2-2 Selected Icing Conditions

Run	MVD μm	LWC (g/m^3)	Velocity (m/s)	Temperature ℃	Spray Time min
2	20	1.0	67.1	-6.42	6
5	20	1.0	67.1	-28.65	6

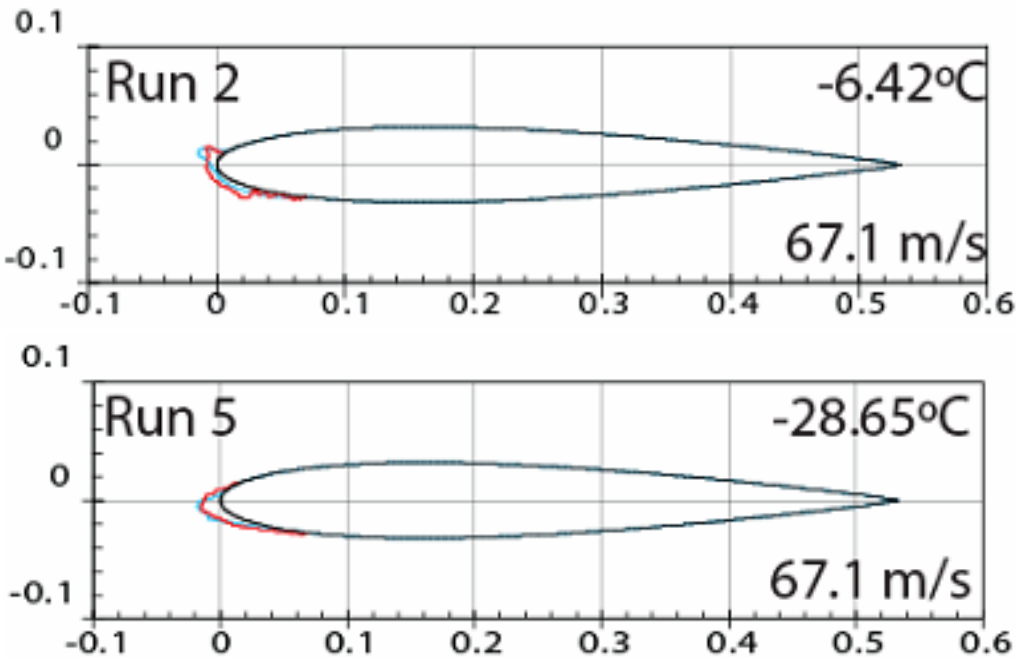

Figure 2-3 Ice Accumulated Shape in Higher and Lower Temperature

The air temperature also has a significant effect on heat flux of thermal ice protection systems. Higher temperature needs less heat flux and lower temperature requires more heating power. More power is used to heat the skin surface so that the surface temperature can reach above freezing point at lower temperature. For example, electro-thermal de-icing system is usually designed with different operation modes according to the Outside Air Temperature (OAT).

2.2.2 Liquid Water Content

Liquid Water Content (LWC) is defined as the mass of liquid water droplets within a unit volume of cloud [2, 6]. Its unit is often given as grams of water per cubic meter of air (g/m^3). A higher LWC results in more water droplets impingement on airframe surface, leading to more severe ice accumulation. Thus it is one of the most significant atmosphere icing parameters.

LWC is considered as a significant parameter affecting aircraft icing. Hansmann reported "high LWC implies a greater urgency and therefore severity of icing encounter" [7]. He also pointed out "higher LWC is to cause the ice accretion to transition from rime to mixed icing due to the higher impinging water load on the icing surface". Figure 2-4 below shows the effects of LWC on ice shapes [8]. From the figure, it is clear that the amount of ice formation increases significantly from a smooth outline to a horn with the LWC rising from 0.25 to 1.00 g/m^3. The icing amount increase and also the ice shape change lead to much more adverse effects on aircraft performance.

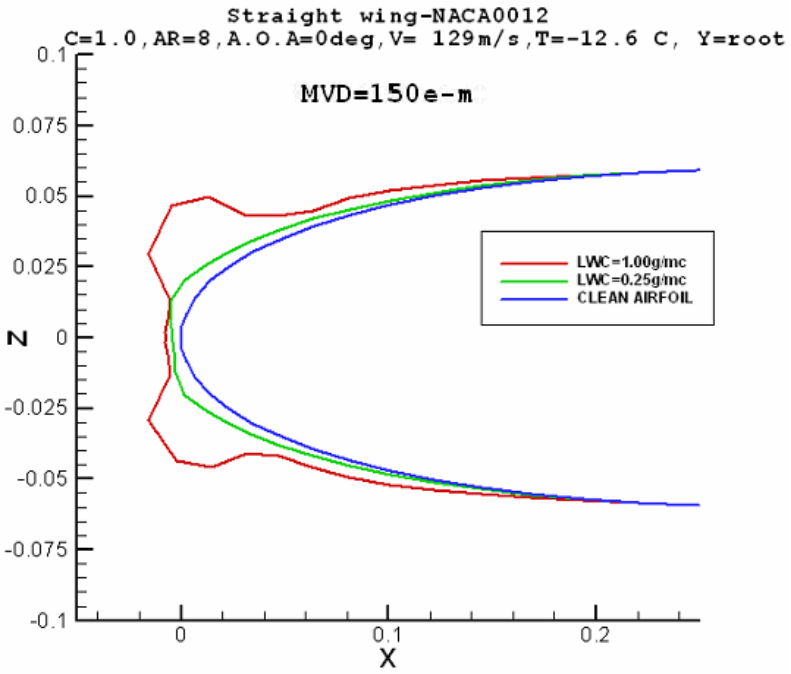

Figure 2-4 Effects of LWC on ice shapes

Moreover, for evaporative anti-icing systems, all the water collected should be evaporated to keep the icing surface dry. So much more energy is required at high LWC. Table 2-3 gives the power required for an inlet anti-icing system to illustrate the relationship between power required and LWC [9]. It is very evident that when atmospheric conditions have higher LWC, even when other parameters are fixed, the power demand is greatly increased. Because of this basic phenomenon, it is beneficial to determine the critical icing conditions for good ice protection system design.

Table 2-3 Power Required and LWC

Altitude/feet	2,2000	2,2000	2,2000	2,2000
KCAS	243	243	160	160
OAT/℉	-22	-22	-22	-22
MVD/micro	20	20	20	20
LWC/(g/m^3)	0.975	0.14	0.975	0.14
Q_{REQD}/(W/in)	48.9	44.5	43.3	39.2

In addition, high LWC creates another problem with high possibility of water droplet runback. It is more difficult for all the large amount of ice to freeze in a short period of time, which can result in the residual water running back to the downstream surfaces and refreezing again. This enlarges the icing zones. Due to the runback ice accumulation, one measure should be considered is to expand the protective area to cover as large area as possible.

2.2.3 Droplet Diameter

The size of water droplets is presented by diameters. Water droplets in the atmosphere have very different diameters, varying from several micrometers to hundreds of micrometers, see Figure 2-5. This raises a question about how to determine the average diameter of droplets in a cloud. Medium Volume Diameter (MVD) is a good solution in icing calculation and IPS design. MVD is defined as the diameter which

divides the total water volume in half so that half the volume is in larger droplets and half the volume in smaller droplets [2, 6].

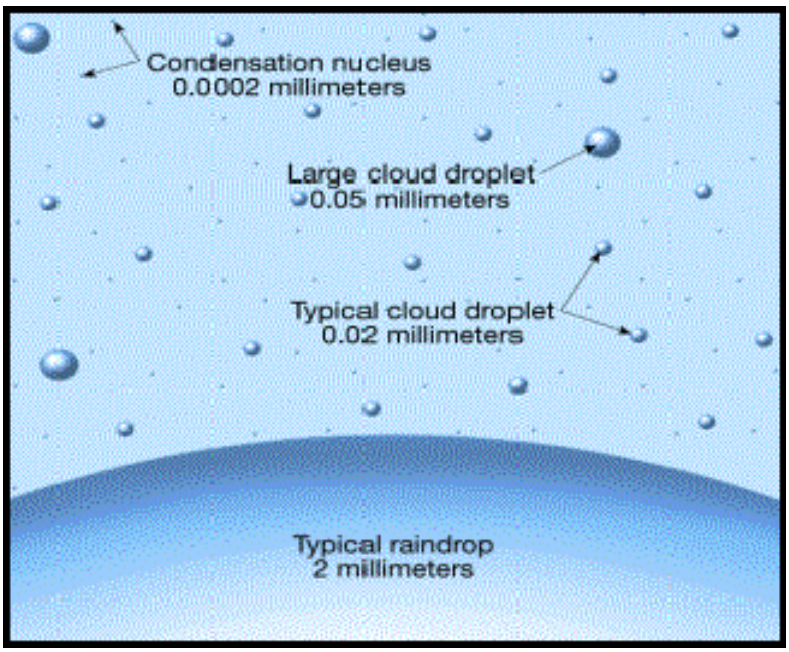

Figure 2-5 Water Droplets in Cloud

Due to the variability of water droplet size, a principle is required to define the water droplets distribution. Langmuir droplet distribution provides us with a universally agreed solution [6], which is the ratio of drop diameter to MVD. Droplets are divided into seven groups, and each group represents a symmetrical distribution of the percentage, which is normalized by the MVD, see Table 2-4, where d indicates the droplet diameter and d_0 is the MVD. The Langmuir D Distribution has the most common application [10, 11, 12, 13].

Table 2-4 Langmuir Droplet Distribution

LWC%	A	B	C	D	E
5	1.00	0.56	0.42	0.31	0.23
10	1.00	0.72	0.61	0.52	0.44
20	1.00	0.84	0.77	0.71	0.65
30	1.00	1.00	1.00	1.00	1.00

20	1.00	1.17	1.26	1.37	1.48
10	1.00	1.32	1.51	1.74	2.00
5	1.00	1.49	1.81	2.22	2.71

Normally, MVD of 20 micrometers, is adopted for aircraft icing and ice protection system design. The Langmuir D Distribution of 20 micrometers MVD is shown in Table 2-5 to give an example, where the total LWC is 0.5g/m^3.

Table 2-5 Langmuir D distribution of 20 Micrometers MVD

d	d1	d2	d3	d4	d5	d6	d7
MVD	20						
Diameter	6.2	10.4	14.2	20	27.4	34.8	44.4
Total LWC	0.5						
LWC	0.025	0.05	0.1	0.15	0.1	0.05	0.025

Droplets size is subject to increase with cloud height rising. Reference [14] displays a curve demonstrating the relationship between diameter and altitude, see Figure 2-6. From this figure, it can be also seen the effects of altitude on temperature and LWC.

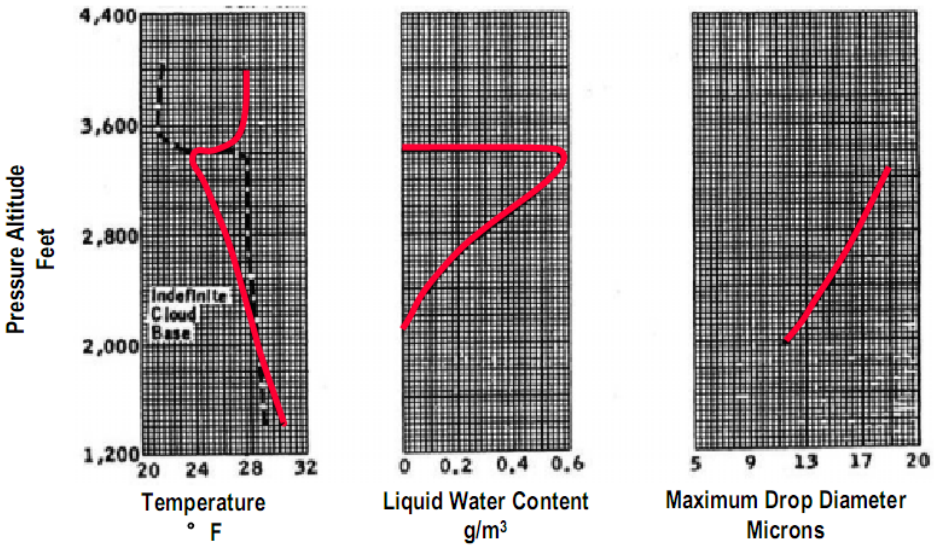

Figure 2-6 Meteorological Parameters Variation with Altitude

Droplet diameter has significant impact on ice shapes. Large droplets are subject to impinge on more extensive surface area due to large inertia while small droplets are likely to deviate from the original trajectory. This is illustrated in Figure 2-7 [15], where V=180 knots, Ts=15.5°F, LWC=0.6 g/m^3 and AOA= 2.5°. This diagram shows the effects of droplet diameter on surface icing extent. It is clearly seen that larger droplets cover more surface and the impingement limit is farther.

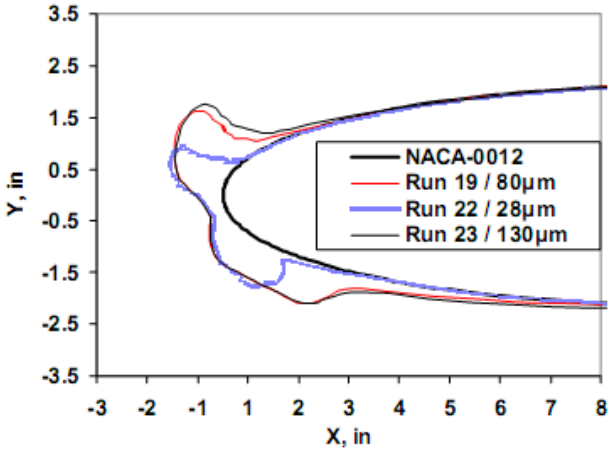

Figure 2-7 Effects of MVD on Ice Shapes

Furthermore, larger droplets may cause ice accumulation beyond the ice protection system. After ice removal, ice ridges can form easily, which has significantly hazardous impacts on aerodynamics. Thus, the IPS designers should consider the coverage of ice protection in order to minimize these adverse effects.

From Figure 2-7, it can be seen the droplet diameter of 80 and 130 micrometers, which belong to Supercooled Large Drops (SLD). SLD is defined as liquid droplets with diameters greater than 50 micrometers below 0 ℃ in freezing rain or freezing drizzle conditions. Although there are no certification requirements existing for IPS design and approval in large drop icing conditions, air accidents that have happened are reinforcing the need for the FAA to address SLD in icing certification [16]. The ATR-72 crash in Roselawn, Indiana on 31st October 1994 is the original report of air crash caused by SLD. The aircraft was the American Eagle Flight 4184, which was

planned to fly from Indianapolis International Airport, Indiana to O'Hare International Airport, Chicago. In this accident, all were killed on the plane including 64 passengers and 4 crews. The main reason is thought to have been a ridge of ice that accreted beyond the de-icing boots causing loss of control. For more details see Reference [17].

Due to the severe icing conditions caused by SLD, numerous pieces of research have been conducted. The research objectives normally focus on three aspects. First of all, the characteristics and properties were investigated, such as distortion, breakup and splashing [18,19]. Secondly, has been taken to simulate the ice shapes generated in SLD icing conditions [20]. Finally, the effects of SLD ice accretion on aerodynamics were studied [21, 22].

2.2.4 Cloud Extent

Cloud extent is defined as both horizontal extent and vertical extent. The primary effect on aircraft icing is the amount of ice buildup. Basically, the more flight time an aircraft spends in longer cloud extent the higher the amount of ice is accumulated on airframe components. So cloud extent is one of the important atmosphere parameters.

As discussed in Chapter 2.1, stratiform cloud is a type of cloud with horizontal distribution. The horizontal size is much larger than vertical size. Normally the height is less than 2,000 meters while the coverage may reach to hundreds of kilometers. Cumuliform cloud has the similar size level in vertical distribution and horizontal distribution. The horizontal extent of cumuliform cloud is usually below 3.7~11 kilometers.

2.3 Meteorology Design Conditions

FAR Part 25, Appendix C provides the cloud parameters as the aircraft icing meteorology design specification [23]. Two icing conditions are used for approval of

aircraft icing and ice protection equipments in flight: continuous maximum and intermittent maximum icing conditions. Aircraft must be able to operate safely in these atmosphere conditions.

In Appendix C, “The maximum continuous intensity of atmospheric icing conditions (continuous maximum icing) is defined by the variables of the cloud liquid water content, the mean effective diameter of the cloud droplets, the ambient air temperature, and the interrelationship of these three variables”. Continuous maximum icing is related to stratiform clouds, whose LWC is relatively lower. The correlation of the meteorological parameters is shown in Figure 2-8[23].

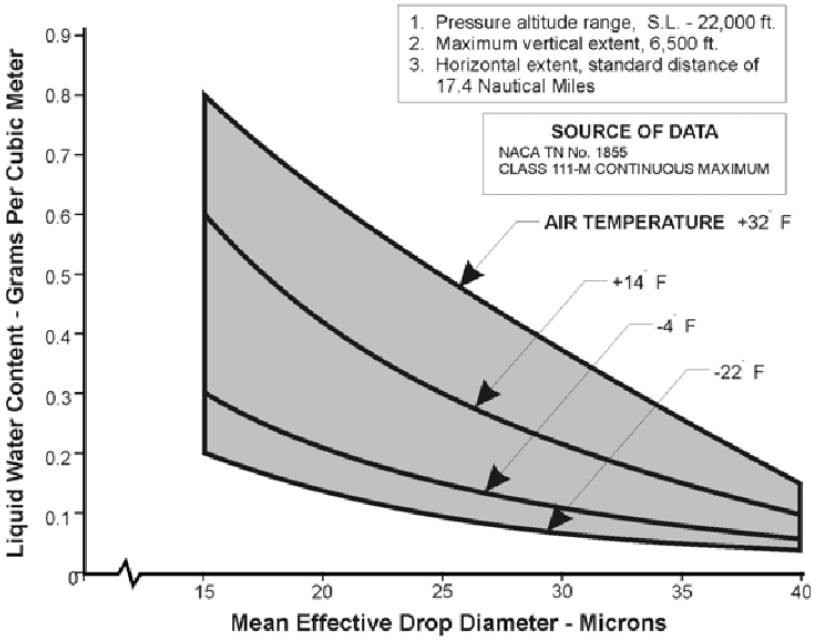

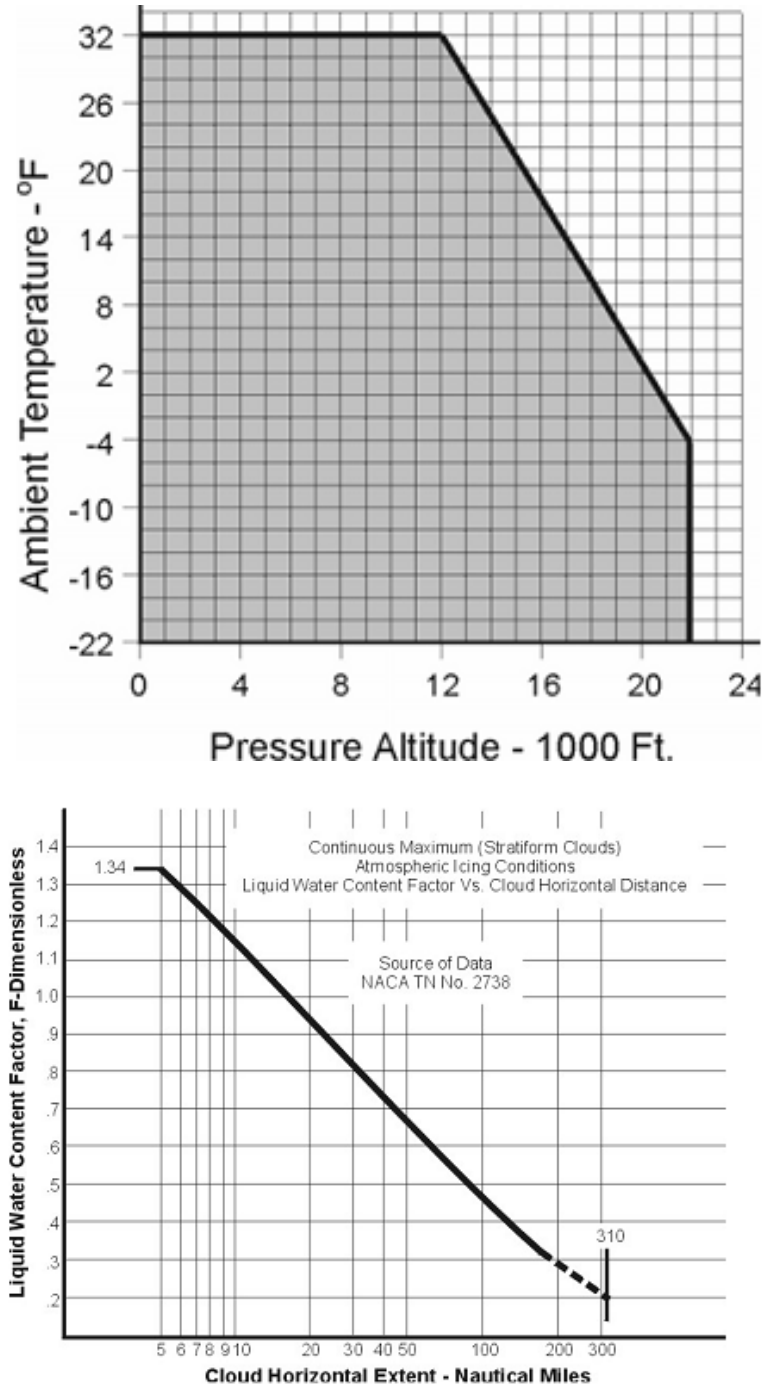

Figure 2-8 Continuous Maximum Icing Conditions

In Appendix C, “The intermittent maximum intensity of atmospheric icing conditions (intermittent maximum icing) is defined by the variables of the cloud liquid water content, the mean effective diameter of the cloud droplets, the ambient air temperature, and the interrelationship of these three variables”. Intermittent maximum icing is related to cumuliform clouds, whose LWC is relatively higher. The correlation of the

meteorological parameters is shown in Figure 2-9[23].

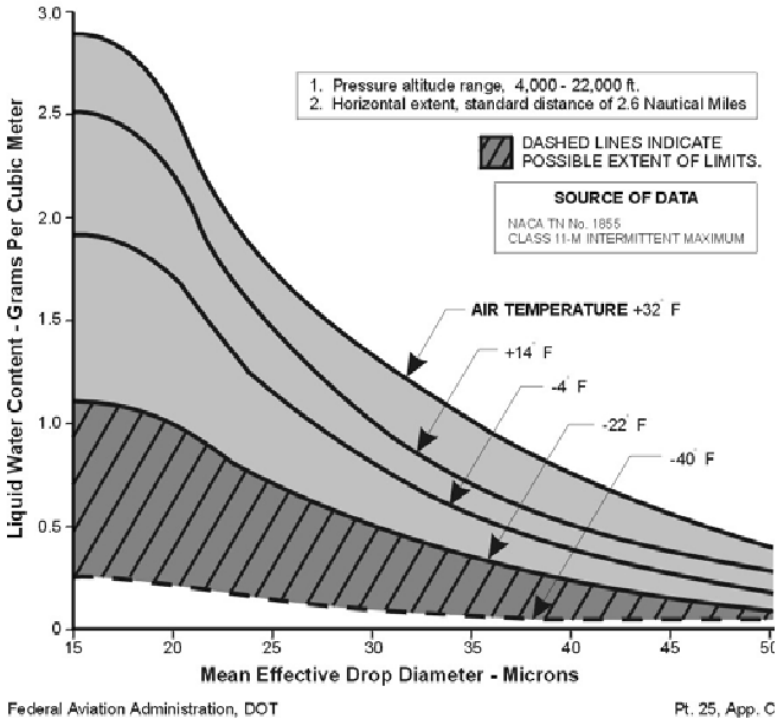

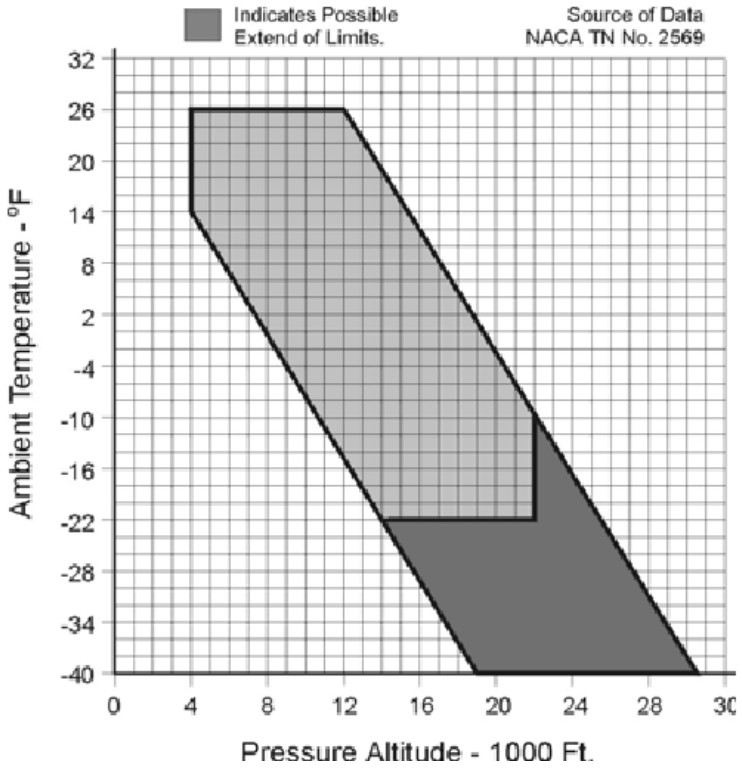

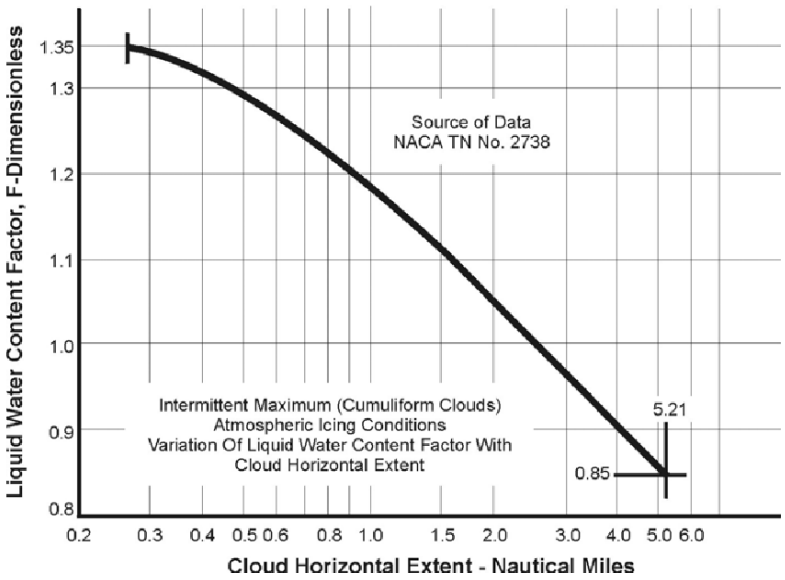

Figure 2-9 Continuous Maximum Icing Conditions

The Appendix C of CS-25 also gives the same icing conditions as mentioned above [24].

2.4 Icing Detection

The detection of icing conditions is extremely necessary to aircraft safety. The icing information alerts the flight crews to activate the ice protection system or to escape from the icing conditions. Thus the detrimental effects of ice accumulation on aircraft safety can be minimized. Flight Icing Detection Systems (FIDS) are available to provide aircraft icing information to the flight crews. FIDS can be categorized into Advisory Flight Icing Detection System (AFIDS) and Primary Flight Icing Detection System (PFIDS) [25].

The AFIDS provides an advisory alert to annunciate the presence of icing conditions. However, the flight crew should not use an AFID as the only mean for icing condition detection. It must be used with other methods to determine the IPS activation. Some typical methods include: total air temperature, visible moisture criteria, visible ice accretion and specific airframe ice accretion thickness, which should be defined in the Aircraft Flight Manual (AFM) [25].

A PFIDS provides aircraft icing alert to the flight crew. In a primary system, the IPS is activated based on the PFIDS alert. The PFIDS can be divided into two categories: primary automatic or primary manual [25]. In a primary automatic system, the FIDS automatically activates the IPS, and the flight crew activates the IPS manually by primary manual system alerts.

In the AFIDS, various means are employed together to determine the ice accretion on the aircraft. So the alert message is relatively reliable and accurate. However, because of the responsibilities on monitoring icing conditions through multi-method, the flight crew's workload is increased. In the PFIDS, the pilot judges the presence of ice accumulation based on the detection system. Although the workload is lighter, once the system fails without warning message, it may be too late for the aircraft to activate IPS or evade icing atmosphere after the flight crew senses the ice accretion. Therefore, higher reliability is demanded for the PFIDS.

Table 2-6 Contrasts among Different Icing Detecting Technologies

Technologies	Basic Principle	Advantage	Drawback
Vibrating Probe	Vibrating frequency decreases while icing	Widely used; Low power consumption; Reliably; Stable performance	Detecting ice conditions indirectly
Hot Wire	Ice unfreezes at a constant temperature	High detecting accuracy (0.13mm)	Cannot distinguish ice thickness
Pressure Array	Pressure decreases while ice accretion on holes	Simple working principle	The holes to be contaminated easily; Not widely used
Light Beam Interruption	Light degree changed with the ice accretion	Sensitive as little as 0.13mm	Cannot determine the thickness of ice
Ultrasonic Wave	Measure ice thickness using ultrasonic waves	Small; Light weight; Measure ice shapes	Need certification to apply on civil aircraft

In order to detect aircraft icing, ice detectors are available in several types in FIDS. Currently icing detecting technologies include: vibrating probe, hot wire, pressure array, light beam interruption and ultrasonic waves. The contrasts among different

icing detecting technologies are shown in Table 2-6 [31].

2.5 Conclusions

Through literature study, the key points of aircraft icing meteorology are summarized above, including cloud types, meteorological parameters, meteorology design conditions and icing detection. This research is helpful to get preliminary understanding of aircraft icing meteorology.

Two types of clouds are surveyed, stratiform clouds and cumuliform clouds. Stratiform clouds distribute widely with lower LWC, so the icing intensity is relatively weaker. However, due to its widely horizontal distribution, the possibility of long time flight in stratiform clouds may result in thick ice accumulation. So it is not advisable to fly in stratiform cloud for a long period of time. LWC of cumuliform clouds is much higher, which results in more severe icing. Because of its vertical type, it is possible for aircraft to exit from cumuliform clouds by changing the flight route.

The significant icing parameters, such as air temperature, water droplet diameter, liquid water content and exposure time in clouds, are investigated to express influences on icing and ice protection. Temperature directly determines whether ice will form on the aircraft surfaces. Rime ice accumulates at a colder temperature while at a warmer temperatures glaze ice accretes. In addition, a higher temperature needs less heat flux for ice protection system. Larger droplets, higher LWC and more extensive icing cloud can raise more critical ice shape and associate with higher requirements for ice protection system design.

Aircraft icing conditions are categorized into continuous maximum and intermittent maximum icing conditions. Continuous maximum icing condition is related to stratiform clouds and intermittent maximum icing condition is defined in cumuliform cloud. When flying in these icing conditions, icing information provided by ice detection system alerts the flight crews to take measures. FIDS is categorized into

PFIDS and AFIDS. Pilots can get icing information from PFIDS directly, however, in an AFIDS, pilots should determine icing conditions with other means, such as temperature, visible moisture and visible ice accumulation.

3 Aircraft Icing

These aspects should be investigated during ice protection system design: a) Which surfaces need ice protection; b) What is the expected extent of icing on protective surfaces; c) How much icing and what types can be accumulated on protective surfaces. In order to answer these questions, droplet impingement characteristics, ice accumulation and the effects of icing on aircraft are considered in this chapter.

3.1 Droplet Impingement

The amount of accreted ice, the extent of surface protection, and the energy needed to protect the surface from icing depend on droplet impingement. The air stagnation line separates the air flow into two zones, where one is going up and the other going down. In the far field, the water droplet trajectory parallels the air streams. However, when approaching the airfoil, water droplets departure from the air streamlines and strikes on the airfoil because the inertia of water droplets is greater than air, see Figure 3-1[6].

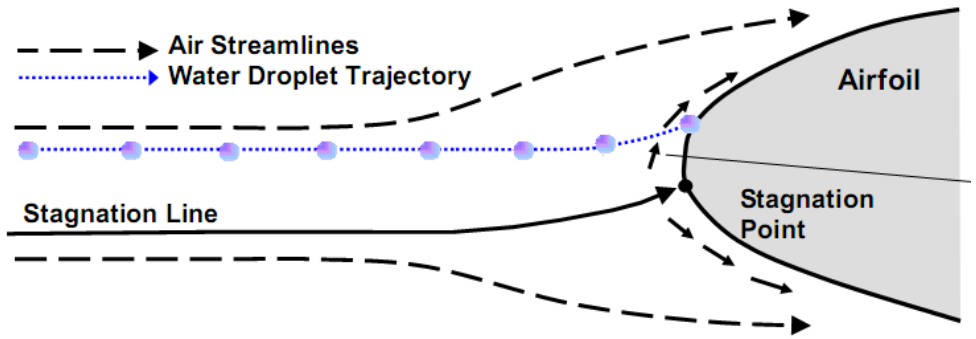

Figure 3-1 Water Droplet Trajectory around an Airfoil

Droplet impingement characteristics are represented by impingement limits, local water catch efficiency and total water catch efficiency.

The impingement limit is defined as “The location farthest aft on a body where water drops impinge. This distance is usually measured as the surface length from the surface’s leading edge” [6]. The limit includes two farthest points, one is on the upper

surface and the other is on the lower surface. These limits are the tangent points of the droplet trajectory to the airfoil (see Figure 3-2[6]). Once the impingement limit is defined, the droplet stroke zone is determined.

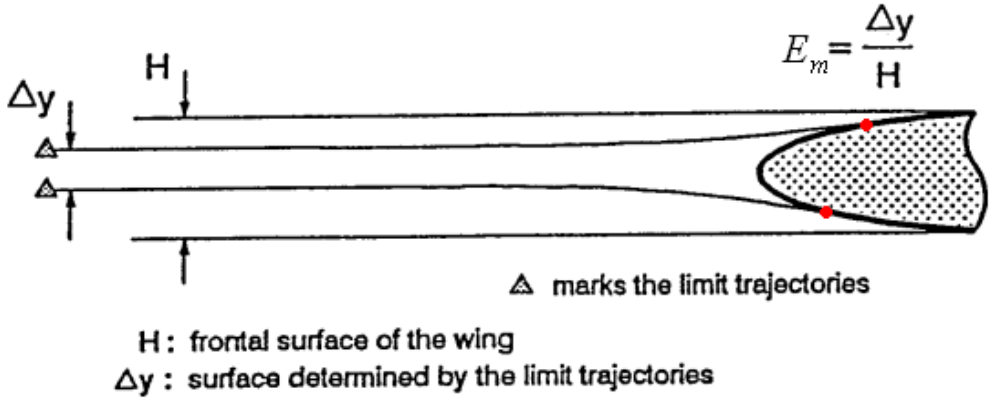

Figure 3-2 Water Droplet Impingement Limit and Catch Efficiency

Water catch efficiency (E_m) is defined as "The ratio of actual water drops mass flux at the surface to the water drops mass flux in the free stream when water drop paths are straight lines" [6]. As shown in Figure 3-2, it is the ratio of Δy to H. From the definition, it is clear that water catch efficiency depends on the limit trajectories. In order to calculate E_m, the trajectories tangent to the airfoil should be investigated.

Local water catch efficiency (β) is defined as "The ratio of dY to ds" [6] (see Figure 3-3[6]). Letting ds approach 0, the value of β is the derivative dY/ds. Therefore, local water catch efficiency represents the distribution of impinged droplets. The distribution is not uniform on the airfoil surface. Normally, β has its maximum value at the stagnation point and the minimum value at the limit. Local water catch efficiency is illustrated by the β curves, from which we can get not only the local water catch efficiency but also the impingement limit. Furthermore, we can determine the water catch efficiency by:

$$E_m = \frac{\int \beta ds}{\int ds}$$

Therefore, local water catch efficiency is the most significant and effective mean to investigate the water droplet impingement characteristics.

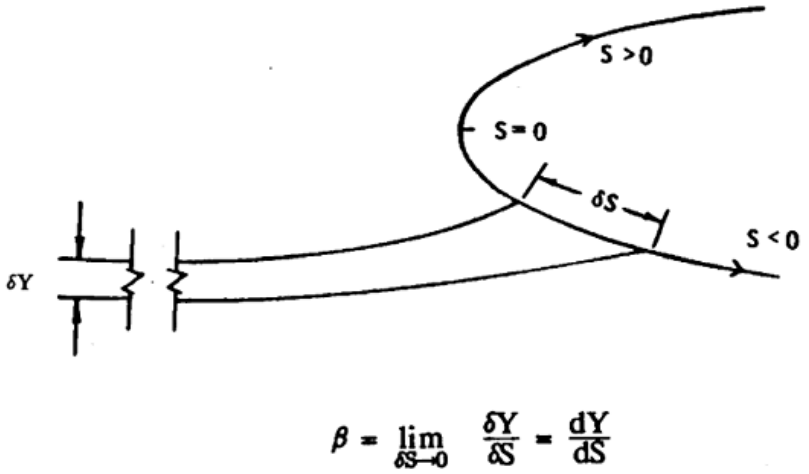

Figure 3-3 Local Water Catch Efficiency

The flight conditions and icing conditions have significant impact on local water catch efficiency, such Angle of Attack (AOA) and Medium Volume Diameter (MVD). Figure 3-4 and Figure 3-5 give the effects of AOA and MVD on local water catch efficiency respectively [26].

Figure 3-4[26] demonstrates the effects of AOA on water catch efficiency. The local catch efficiency goes down from the stagnation point to the two sides. With the AOA increasing, the impingement limit on the upper surface decreases and the lower one rises, which results in the icing zone moving from the upper surface to the lower surface. In addition, the local catch efficiency at the stagnation point decreases.

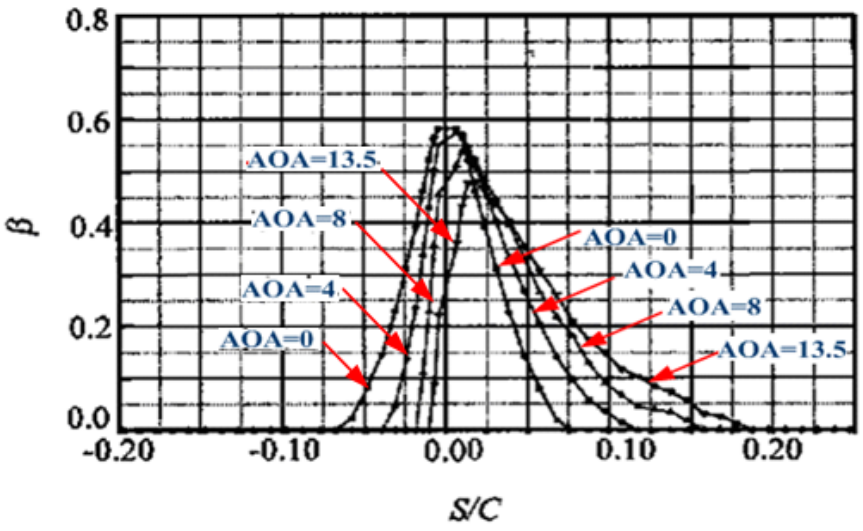

Figure 3-4 Effect of AOA on Local Catch Efficiency

(MVD =16 μm, LW C= 1.0 g/m^3)

Figure 3-5[26] shows the effects of MVD on water catch efficiency. Water droplets with smaller MVD are more subject to the air stream and easily deviate from the original trajectory. While bigger droplets have higher inertia, the air effect on droplet trajectory is less. Thus the impinged zone and water catch efficiency increase with the growth of MVD.

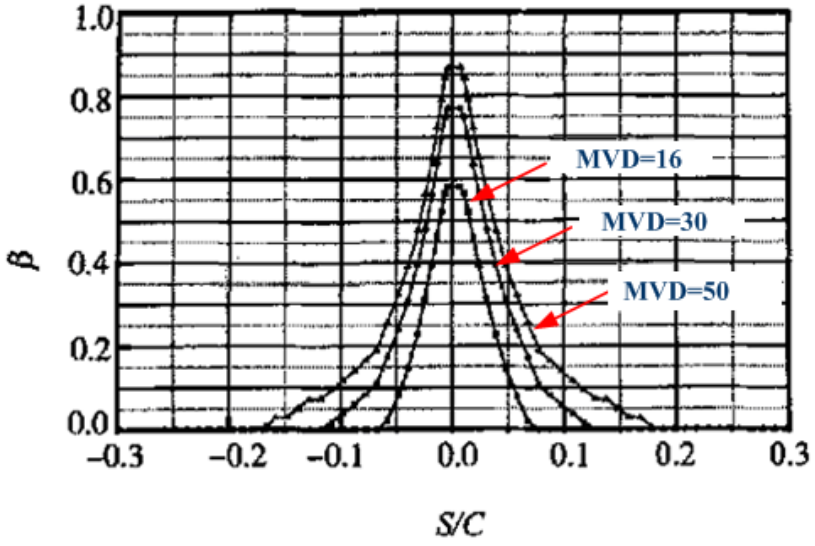

Figure 3-5 Effect of MVD on Local Catch Efficiency

(AOA = 0°, LW C= 1.0g/m3)

3.2 Aircraft Ice Accretion

The amount and rate of icing depend on a number of meteorological and aerodynamic conditions, such as LWC, temperature, droplet diameter, flight velocity and AOA. The effects of the meteorological parameters on aircraft icing have been discussed in Chapter 2.2. Before discussing aerodynamic icing parameters, it will be helpful to introduce the icing intensity.

Icing intensity is defined as the icing rate on the surface. Icing intensity can be divided into four levels, which are light, moderate, heavy and severe [6].

For light icing, the rate of ice buildup is 0.25 inch to 1.0 inch (0.6 to 2.5 cm) per hour (0.1~0.4 mm/min) on the outer wing. The pilot should consider this icing condition. If the exposure time is too long, the pilot needs to activate the ice protection system or evade the icing clouds.

As to moderate icing, the rate of ice accretion ranges from 1 to 3 inches (2.5 to 7.5 cm) per hour (0.4~1.3 mm/min) on the outer wing. The pilot should consider this icing condition as soon as possible and switch on the ice protection systems. Moreover an ice detection system designer should consider the icing speed to determine the output signal with the corresponding ice amount value.

As far as heavy icing is concerned, the rate of ice accumulation is more than 3 inches (7.5 cm) per hour (1.3 mm/min) on the outer wing. If an aircraft flys into such an icing encounter, the pilot should consider exiting from the conditions immediately. Even so, it requires maximum use of the ice protection systems to minimize ice accretions on the airframe.

When operating in a severe icing atmosphere, the ice protection systems are not able to remove the buildup of ice. Also, ice builds up in locations which are not normally prone to icing, such as areas aft of protected surfaces, which is similar to SLD icing conditions. In this situation, it is necessary to exit from the condition immediately.

The definitions of icing intensity are shown in the Table 3-1.

Table 3-1 Definitions of Icing Intensity

Intensity	Rate (inch/hour)	Equivalent Rate(mm/min)	Pilot Response
Light	0.25~1.0	0.1~0.4	Occasional use of IPS equipment may be necessary.
Moderate	1.0~3.0	0.4~1.3	Consider this condition and switch on the IPS
Heavy	> 3.0	> 1.3	Exit from the conditions and switch on the IPS
Severe	-	-	Immediate exit from the icing condition is mandatory.

Besides talking about the icing intensity, it is necessary to discuss ice shapes. Different icing atmospheres and flight conditions cause unique ice shapes, which have an array of differing adverse effects on aircraft flight. The ice shapes can be divided into 3 categories: glaze ice, rime ice and mixed ice [27].

Glaze ice is smooth and generally translucent. Glaze ice results from larger supercooled drops striking a surface at a warmer temperature, thus not rapidly freezing on contact and allowing air to escape. In addition, the rate of accretions is higher. Therefore a horn type shape is often formed. Glaze ice is denser, harder, so it is more difficult to break. It changes the shape of airfoils dramatically and destroys air stream significantly, causing more serious aerodynamic problems. A typical image of glaze ice is shown Figure 3-6.

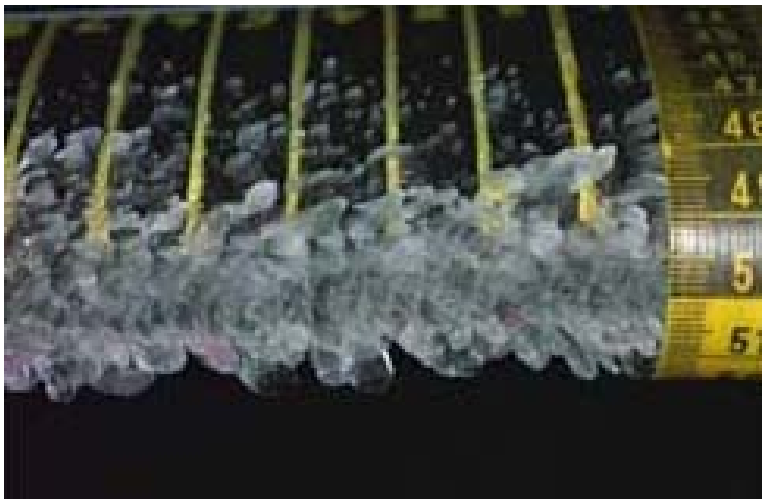

Figure 3-6 Typical View of Glaze Ice

The characteristic appearance of rime ice is rough, milky and opaque. This type of ice occurs at lower temperatures with smaller supercooled drops striking the aircraft surface. The rapid freezing results in a mixture of tiny ice particles and trapped air. So the appearance is opaque and rough. Rime ice typically accretes at a lower rate and forms a more regular shape than glaze ice. A typical picture of rime ice is illustrated in Figure 3-7.

Figure 3-7 Typical View of Rime Ice

Mixed ice is the characteristics of both glaze and rime ice. Different droplet sizes are in cloud, which produces a mixture of clear ice (from large drops) and rime (from

small droplets), known as mixed ice. A typical image of mixed ice is shown in Figure 3-8.

Figure 3-8 Typical View of Mixed Ice

As mentioned above, the effects of the meteorological parameters on aircraft icing have been discussed in Chapter 2.2. Now the effects of flight parameters on aircraft ice accumulation are introduced, including flight speed and AOA.

Airspeed has an effect on the ice shapes. High airspeeds result in temperature increase on the leading edge and a glaze ice with horns may accrete. The effects of airspeed combined with temperature are illustrated in Figure 3-9.

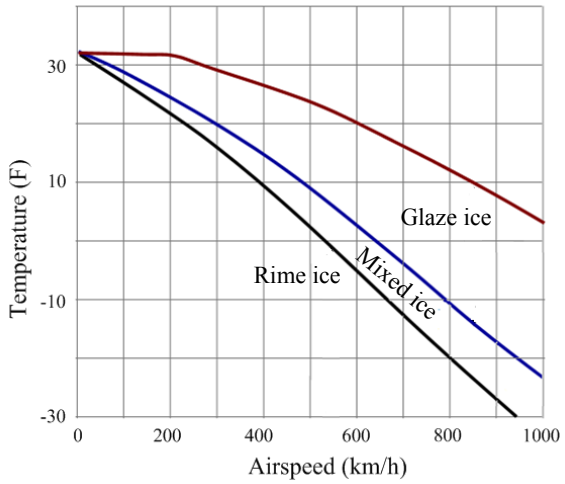

Figure 3-9 Effects of Airspeed and Temperature on Ice shapes

The effect of AOA on airfoil icing is shown in Figure 3-10[8]. When the AOA increases, the icing zone decreases on the upper surface and increases on the lower surface. This is caused by the impingement limit move from upper surface to lower surface with the angle rise.

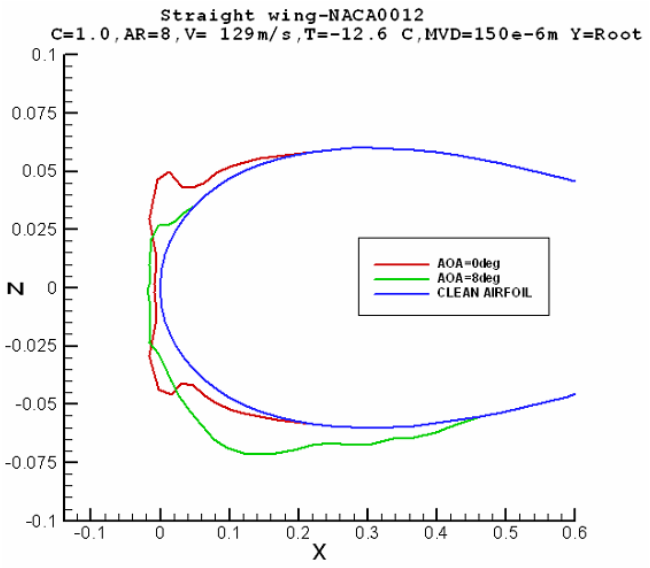

Figure 3-10 Effects of AOA on Ice shapes

3.3 Icing Effects on Aircraft

The leading surfaces of aircraft may catch ice formation during icing atmospheric conditions, including lifting surfaces (wings, empennages), windshields, sensors, nacelle and engines. Different parts have different responses to ice accumulation.

3.3.1 Lift Surface Icing

When ice accumulates on wings and empennages, the aerodynamic performance will degrade and cause maneuverability problems. As shown in Figure 3-11[28], the lift becomes lower and the drag increases due to icing. Furthermore, because of separation of the airfoil upper surface boundary layer, the critical AOA decreases significantly.

The icing effect on maneuverability can not be ignored. Especially during takeoff and landing, horizontal stabilizer icing will deteriorate the maneuverability. For example, on conventional aircraft, the horizontal stabilizer provides longitudinal stability by creating downward lift. With flaps extended during takeoff and landing, the wing centre of lift moves aft, which causes the nose to move down. In order to balance this situation, more AOA of horizontal stabilizers is required. However, in icing encounters, stabilizer icing will result in stall, lift decrease and cause maneuverability problems.

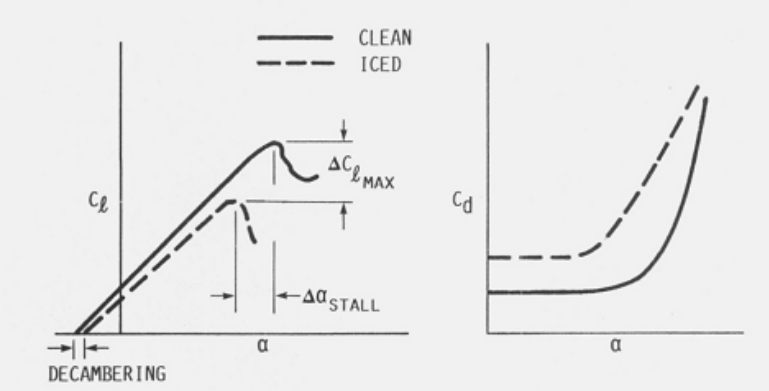

Figure 3-11 Aerodynamic Performance Degradation Due to Icing

3.3.2 Nacelle and Engine Icing

Nacelle inlet surfaces are susceptible to icing, which causes the degradation of inlet aerodynamic performance. Consequently, the inlet air turbulence may lead to engine vibration and propulsion decline, even engine power off. In addition, the ice accumulated on the nacelle may break off and be ingested by the engine. This may damage the engine and cause a serious accident. The rotating fan blades and the spinner can accrete ice and have the similar adverse effects on engine performance and safety. The typical view of nacelle and engine icing is shown in Figure 3-12.

Figure 3-12 Nacelle and Engine Icing

For propeller engines, ice buildup is also very common and can have a significant impact on flight safety. Propeller engine icing may occur on the surface of blades and cowlings. This ice accumulation may lead to a serious loss of thrust, vibrations and engine failure. It will damage the adjacent structure when ice is detached by centrifugal force.

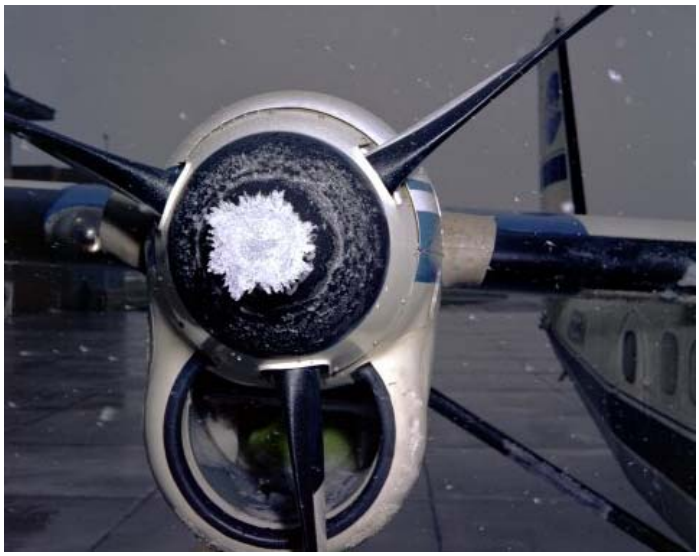

Figure 3-13 Aircraft Icing on a Propeller Engine

3.3.3 Windshield Icing

Windshield icing has little effect on aerodynamics performance, but the visibility of

pilots could be impaired. Thus the pilots are not capable of seeing the outside surroundings clearly and danger may occur during taking off and landing. A typical view of aircraft icing on windshield is illustrated in Figure 3-14.

Figure 3-14 Aircraft Icing on Windshield

3.3.4 Probe Icing

During icing conditions, probes installed on the aircraft exterior surfaces may accrete ice, such as the outside ambient temperature gauge and pitot tubes. For example, the pitot tube can be blocked easily because of ice accumulation in icing encounters. This problem will affect the airspeed indication, and could even result in the loss of airspeed indicating function. It was reported that simultaneous failure of all three pitot tubes because of rime ice formation was one of the factors in the accident of Air France Flight 447 (Airbus 330), which crashed into the Atlantic Ocean on June 1st 2009 with the loss of all 216 passengers and 12 flight crews lost their lives [29]. A typical picture of ice accumulation on a pitot tube is shown on Figure 3-15.

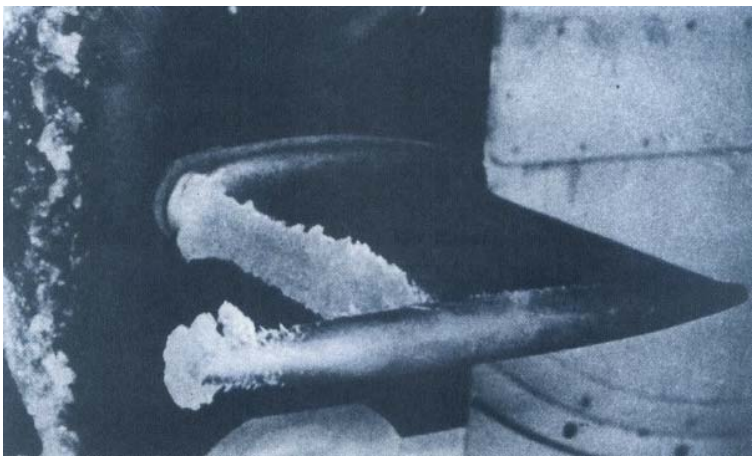

Figure 3-15 Ice Accumulation on a Pitot Tube

3.4 Conclusions

This chapter introduces aircraft icing in terms of droplet impingement characteristics, icing accretion types and icing effects on aircraft. Through the investigation in this chapter, the droplet trajectory of movement, aircraft icing characteristics, aircraft performance degradation and icing effects on flight safety are well understood.

Ice accretion characteristics, protected surface extent and energy distribution of IPS depend on droplet impingement. Local water catch efficiency is the most significant and effective mean to present the water droplet impingement characteristics. Aircraft flight conditions and icing environment have significant effects on droplet impingement characteristics. For example, with AOA increasing, the impingement limit on upper surface decreases and the lower one rises. And impinged zone and water catch efficiency increase with the growth of MVD.

Aircraft icing rate is presented by icing intensity, which can be divided into four levels: light, moderate, heavy and severe. In light and moderate icing conditions, switch on ice protection system is necessary before ice accumulation becomes in excess of the critical amount. However, aircraft should exit from the heavy and severe icing condition immediately even the aircraft is approved for flight in icing conditions.

Three ice shapes are studied, including glaze ice, rime ice and mixed ice. Glaze ice is dense, hard and generally in translucent appearance and may cause more serious aerodynamic problems. Rime ice presents with rough, milky, opaque appearance and regular shape, having less adverse effects than glaze ice. Mixed ice is a combination of both glaze and rime ice characteristics.

Ice is subject to build up on aircraft leading area of lifting surfaces (wings, empennages), windshields, probes, nacelle and engines. Ice accreted on lifting surfaces will degrade aerodynamic performance and cause maneuver problems. Engine and nacelle icing causes the degradation of inlet aerodynamic performance and broken off ice may be ingested by the engine. This may damage the engine and cause serious accident. Ice on windshield impairs the visibility. In addition, the ice buildup may adversely affect the probe's function. So it is essential to adopt effective measures to avoid or reduce the icing adverse effects on aircraft safety.

4 Ice Protection Systems

Ice protection systems work in either anti-icing where ice accumulation is prevented or de-icing where ice is removed once it has formed. Anti-icing is used in the parts where any ice formation accretion is unacceptable, such as nacelle/engine, windshields and probes. De-icing is employed in these areas where ice buildup, with a fixed thickness, has only minor effects on flight safety. Whether it would be reasonable or not to employ de-icing on other icing surfaces (such as wing and empennage) depends on the icing sensitivity. If the wing and empennage can handle some ice accumulation without significant degradation of aerodynamics performance, de-icing is feasible. Otherwise, anti-icing is mandatory.

According to the operation principles, ice protection systems are divided into three categories: thermal, mechanical and fluid ice protection system. Thermal and chemical ice protection systems can operate in either anti-icing or de-icing mode. However, mechanical ice protection systems should only perform de-icing. This chapter will focus on different ice protection systems.

4.1 Fluid Ice Protection Systems

Fluid ice protection systems operate with the principle that the protected surface is coated with a fluid. When striking the surface, the water droplets mix with the fluid to lower the freezing point below the ambient air temperature. Current systems normally use a glycol-based fluid. A typical example is the fluid ice protection system produced by TKS [30]. The fluid system schematic is shown in Figure 4-1[30]. This fluid system is used to prevent ice formation on wings, empennages, propellers and windshields. For the wings and empennages, the laser-drilled titanium panels are installed on the leading edges. As to the propellers, a slinger ring is employed. In front of the windshield, a spray bar is positioned. The glycol-based fluid is pumped to flow over the protected surfaces through the panels, slinger ring and spray bar, keeping the

surfaces free of ice accumulation.

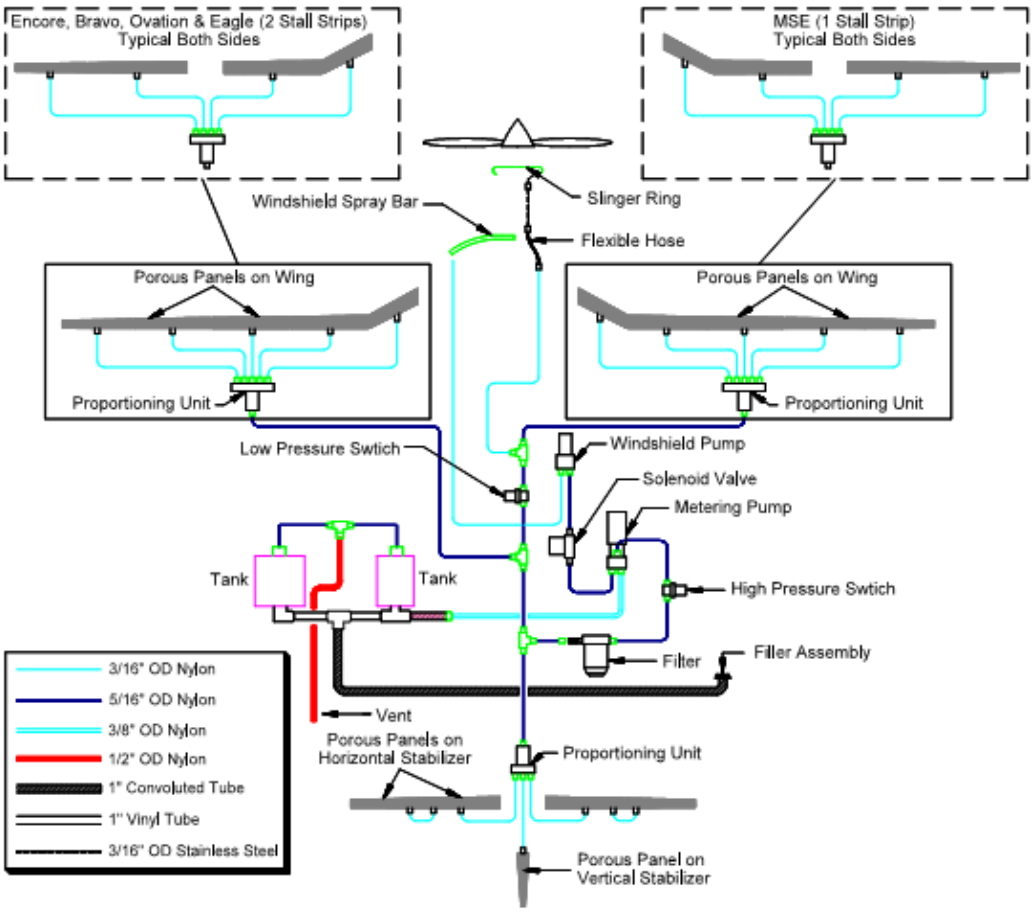

Figure 4-1 TKS Fluid Ice Protection System Schematic

Fluid ice protection systems have good maintainability and high reliability. The components are designed to last the life of the airframe and the pump is the only moving component. These systems have no adverse effects on aerodynamics when anti-icing. In addition, only a small amount of power is required, typically 30 to 100 watts [31]. However, the system has a finite period of ice protection due to the limited fluid supply. Furthermore, the fluid weight reduces the aircraft useful load. Especially during the non-icing weather, carrying such weight may cause higher fuel penalties. The space used to install the fluid tank should be also considered.

4.2 Mechanical Ice Protection Systems

Mechanical ice protection systems only work as a de-icing function. These systems destroy the cohesion between the ice and surfaces. Consequently, the broken ice pieces are blown away by the air stream. The distinct advantage of such systems is that required de-icing power is considerably lower than other systems. However they require a sufficient thickness of ice to function efficiently.

4.2.1 Pneumatic Boot De-icing System

Pneumatic boot de-icing systems destroy ice accretion mechanically by a flexible rubber boot. The ice is broken up by periodically inflating and deflating the tubes. Aerodynamic forces then blow the removed ice particles away. A typical pneumatic boot is shown in Figure 4-2.

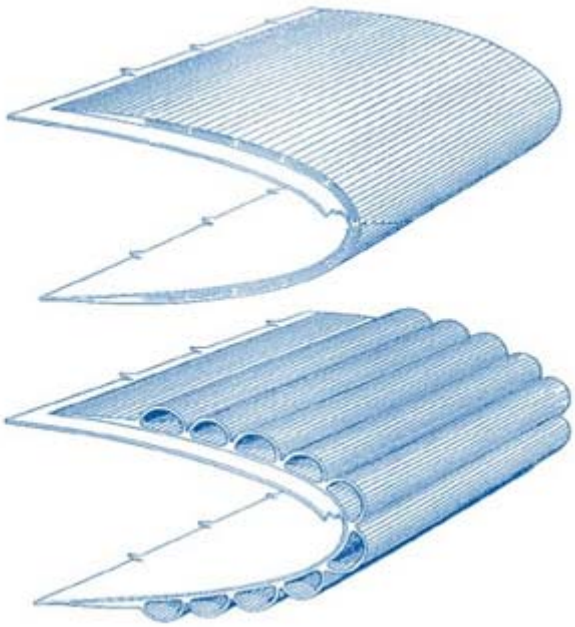

Figure 4-2 De-icing Pneumatic Boot

In addition to the boots, the pneumatic system is comprised of primary components including a regulated pressure source, a vacuum source, and an air distribution system and other miscellaneous components including a solenoid, check and relief valves, air

filters, control switches and timer, fuses and circuit breakers [31]. The regulated pressure source is used to expand the boot for removing the ice buildup. The vacuum source is essential to insure positive deflation and keep the tubes collapsed during non-icing conditions to minimize the aerodynamic penalty. A typical pneumatic boot de-icing system schematic is shown in Figure 4-3 [31].

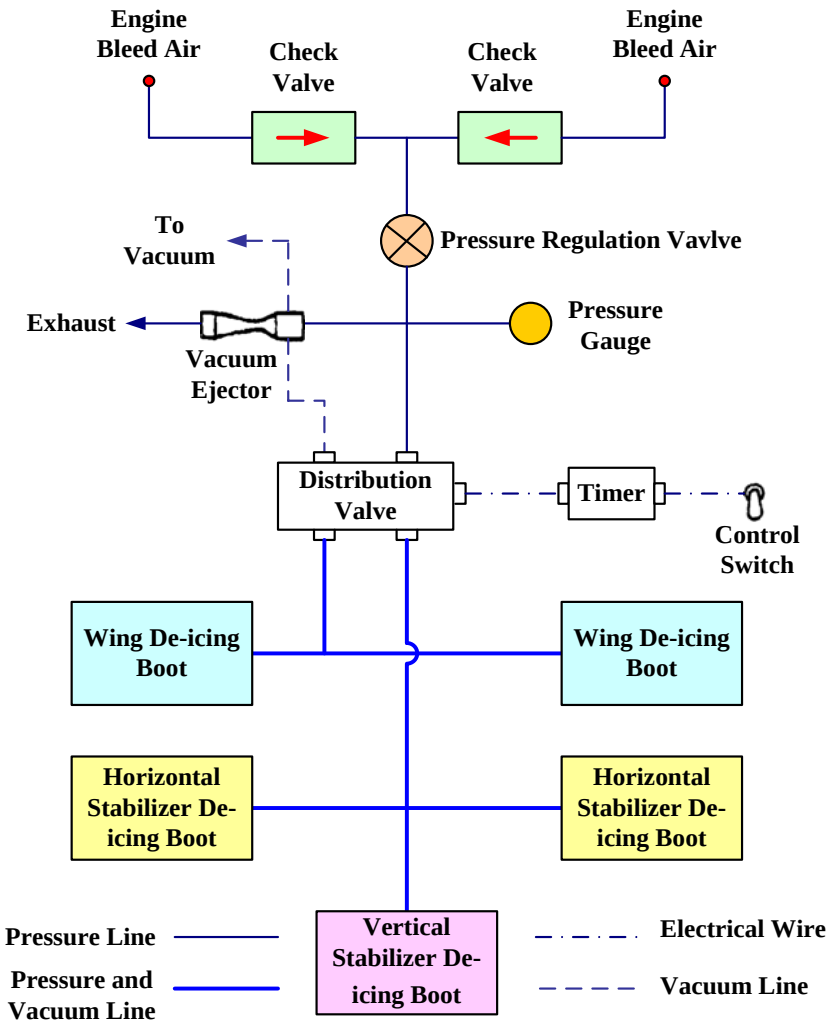

Figure 4-3 Typical Pneumatic Boot De-icing System Schematic

A typical pneumatic system utilizes engine bleed air as the pressure source, used for boot inflation. For safety reasons, a regulation valve is designed to limit over pressure. The regulated bleed air is routed to the air ejector which provides vacuum for boot deflation. The distribution valve has two boot distribution ports, one is used to inflate and deflate the wing boots and the other is used for the empennage boots.

Generally, the average ice thickness allowed is about 0.5 inches (12.7 mm) before the system is switched on. This thickness is determined by the type of boots, leading edge contour, air speed, atmospheric conditions and drag characteristics [31]. Furthermore, in order to improve the function efficiency, the pneumatic boots should inflate and deflate rapidly. To achieve this objective, typically 5 to 6 seconds are required to reach full pressure. During a moderate icing encounter, it is suggested the operation cycle with every 60 seconds, while for light icing conditions, 3 to 4 minutes ice accretion would be acceptable [31].

Pneumatic boot de-icing systems have been utilized on aircraft for many years, and the repair, inspection, maintenance and replacement are well understood. The system weight and power requirements are minimal. However, pneumatic boot de-icing systems have inherent limitations:

a) The rubber boot deteriorates with time and engine oil deposits may damage the material. Thus periodic inspections are required.
b) Aerodynamic drag penalty is inevitable when the boots are inflated, so it is not suitable for higher speed aircraft.
c) Ice pieces shedding from the boot surface may damage the aft airframe, especially the aft engines and propellers.
d) Aircraft pilots need a certain degree of skill to activate the pneumatic boot de-icing system because of safety and efficiency concerns. If the thickness of ice is too thin, activating the system may cause ice bridge, which is ice formation over the boot. This ice bridge can not be removed by subsequent boot inflations. So it is not easy for a pilot to decide the best time to switch on the systems due to the minimal de-icing thickness requirements.

4.2.2 Electro-Impulse De-icing System

Electro-Impulse De-icing System (EIDS) performs its functions using electromagnetic forces, which cause very small but extremely rapid deflection of the skin surfaces.

The principle is shown in Figure 4-4 [31]. The ribbon-wire coils are the primary components of EIDS, which are rigidly supported inside the protected surface. The coils are installed by a small gap separated from the skin inner surface. Capacitors are discharged through the coils, and then a strong electromagnetic field forms and collapses, inducing eddy currents in the protected surface. The eddy current and coil current fields are mutually repulsive, causing the skin surface to flex and destroy the ice accumulations. Typically, the peak force on the skin is 1780 to 2220 Newtons and the surface deflection is lower than 0.25 mm, and the discharge time is less than one-half millisecond in duration [31].

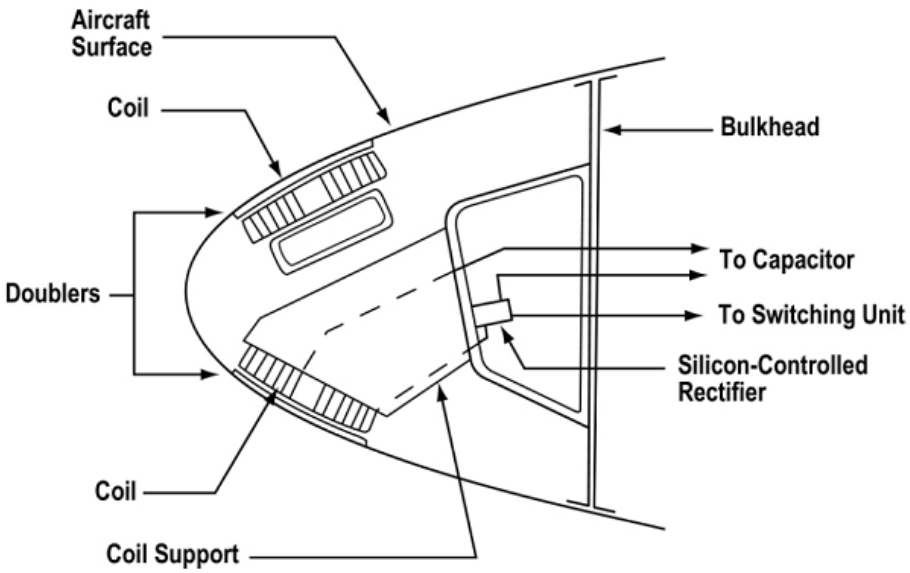

Figure 4-4 Impulse Coils Installed in a Leading Edge

The basic circuit of EIDS is shown in Figure 4-5[31]. The resistance and inductance in the circuit is very low so that the capacitor discharges very rapidly. A remote trigger signal to thyristor is used to activate the energy discharge from the capacitor. Because the thyristor has diode properties, the current in the circuit is similar to the initial positive current response of an underdamped series RLC circuit. When the current approaches zero and attempts to go negative, the thyristor re-opens the circuit, which leads the capacitor to be reversed-charged. Reverse-charging may reduce capacitor life, so a clamping diode is paralleled across the capacitor.

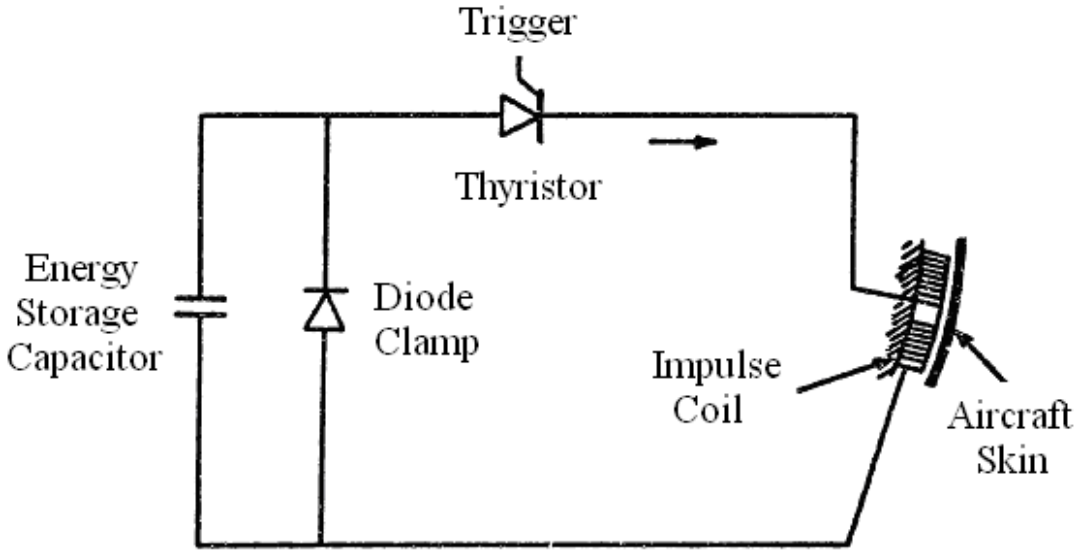

Figure 4-5 Basic Circuit of EIDS

The capacitor units supply 2 or 3 successive pulses during EIDS operation. Such successive pulses are typically separated by 2 to 4 seconds required to recharge the capacitors. The spanwise extent of each coil in the wing leading edge depends on the skin structure properties. Normally, the distance is 0.5 meters. Once the EIDS is activated, the coils receive the successive pulses subsequently. After the first coil discharge, the capacitor is then switched to another coil, and then to another until it finishes a cycle around the aircraft. The cycle period should be less than the time during which ice accumulation on the protected surfaces is acceptable.

Coil arrangement in the protected surface is shown in Figure 4-6[31]. The coils use a common supply cable and each coil has its own thyristor. The thyristor receives a triggering signal from a program switching to activate the coil consequently.

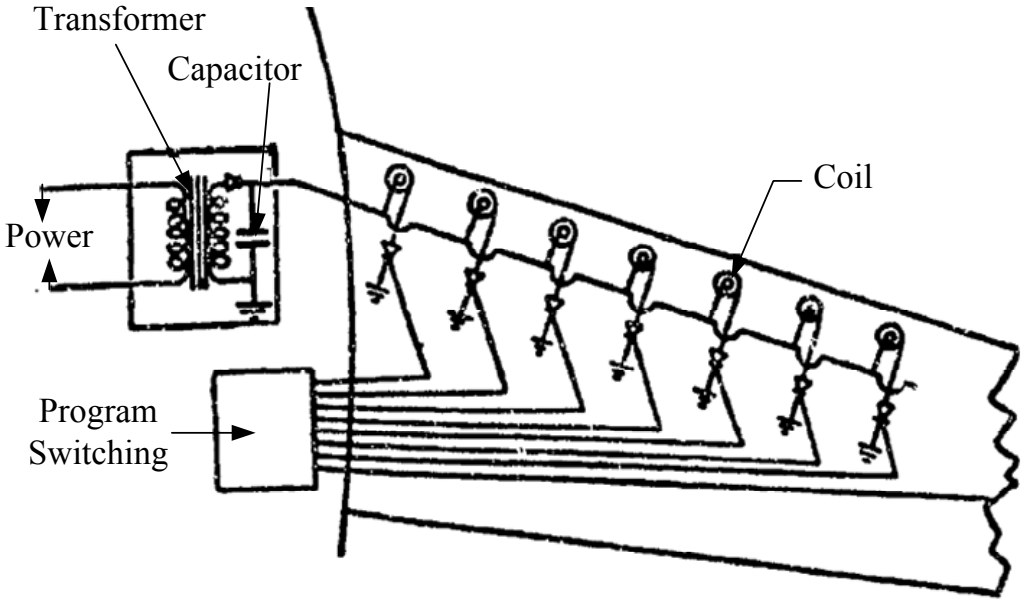

Figure 4-6 Typical Electro-Impulse De-icing System Arrangement

As a type of mechanical ice protection technology, the power required for EIDS is very low, only 1% of that required for a thermal anti-icing system [31]. Besides that, EIDS is a reliable de-icing method, after an impulse, only light residual ice remains on the surface. In addition, EIDS has no adverse aerodynamic effects unlike pneumatic boot system because the surface deflection is too small to affect the air stream. The maintenance workload is very low as there are no moving parts included in the system. It is a promising de-icing technology, but the following aspects should be investigated before its use in engineering applications:

a) Since the electromagnetic forces are periodically applied on the skin and coil supports, then fatigue is possible. Fatigue of aircraft skin is especially important as it may damage structural integrity and endanger the flight safety.
b) Electromagnetic interference should be considered. The discharge of capacitors producing transient electromagnetic fields may cause unintended signals in communication, control or navigation equipments.
c) Because the EIDS is an electrical system, a lightning strike may disable the system. The possible adverse effects of lightning strikes should be tested.

d) The application of EIDS originated in the former USSR aircraft, such as IL-82 and IL-96. However, these aircrafts are not civil transporters, in order to obtain certification for this new type system for civil aircraft, the high cost of certification should be considered.

4.2.3 Electro-Magnetic Expulsion De-icing System

The Electro-Magnetic Expulsion De-icing System (EMEDS) is similar to EIDS, using the electromagnetic principles. The EMEDS is detailed in the US patent 6102333 [32]. The system employs electromagnetic actuators mounted inside the airfoil to remove ice accumulation, see Figure 4-7[32].

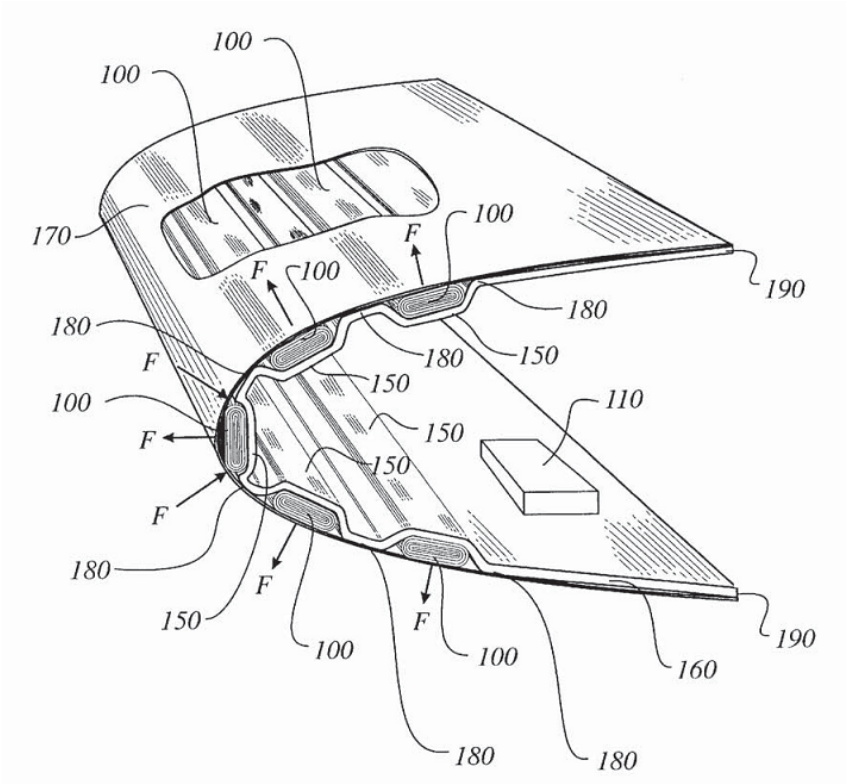

Figure 4-7 Electro-Magnetic Expulsion De-icing System of a Typical Airfoil

The actuator (100 in Figure-4-7) is mounted in the airfoil leading edge, including conductive strips and dielectric sheet. The conductive strips are fabricated on a flexible dielectric sheet to be wound into coil and then shaped into a flattened elongated tube. The dielectric sheet is used to prevent electrical shorting between the

conductive strips. The axis of the coils is coincident to the longitudinal axis of the flattened elongated tube. The longitudinal displacement between coil layers is constrained by this flattened elongated tube. Typically, the coil tubes are installed within the corrugated channels (150) of the housing (160). The housing is usually covered by semi-rigid skin, such as stainless steel or aluminum, which also has the function of corrosion resistance and lightening protection.

The driver electronics are designed for each actuator or actuator group, including a capacitive storage bank, a silicon control rectifier switch (SCR), a charging circuit and a control module, see Figure 4-8[32]. The charging circuit is used to charge the capacitive storage bank. When EMEDS is activated, the control module triggers the SCR and then causes an instantaneous discharge through the actuators.

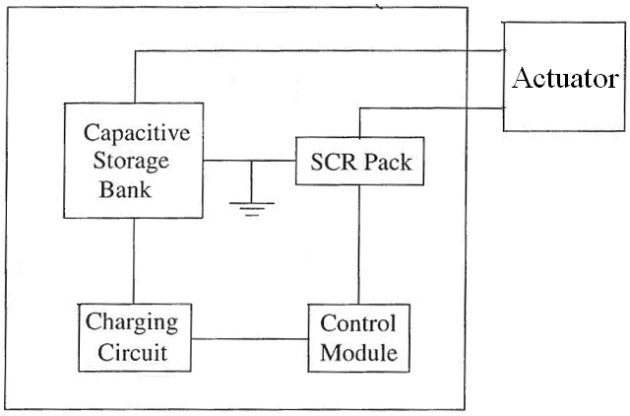

Figure 4-8 Driver Electronics Diagram

Discharge of capacitor causes an instantaneous current flow within the actuator, see Figure 4-9[32]. The directions of current paths are mutually opposite, illustrated by arrows. Particularly, current in the top windings flows in one direction, while current in the low windings travels in the other directions. Therefore magnetic fields with different directions rise, resulting in repulsive electromagnetic force. This force makes the coil expand from flattened shape to a more oval shape rapidly, exerting an impulsive force on the semi-rigid skin with a small deflection. The ice accumulation on the skin is then removed by the skin deflection.

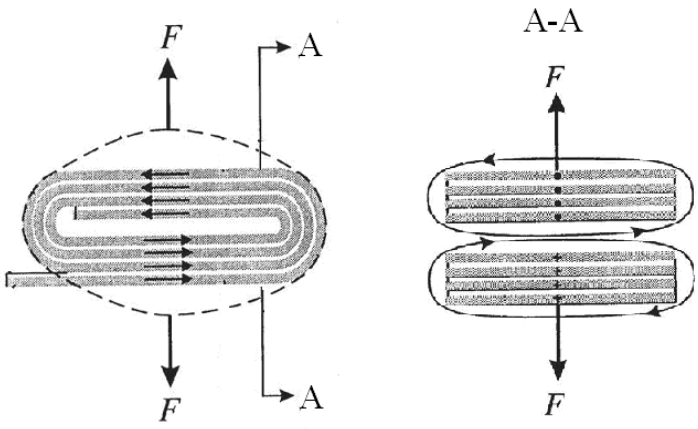

Figure 4-9 Actuator Cross Section

Cox & Company has developed this EMEDS system, including an electronic de-icing control unit, an energy storage bank and a leading edge assembly [33]. The schematic is illustrated in Figure 4-10[33]. The electronic de-icing control unit is used for timing and system control. The energy storage bank can deliver high current electrical pulses. The leading edge assembly consists of actuators mounted in an airfoil-shaped structure with a metal erosion shield.

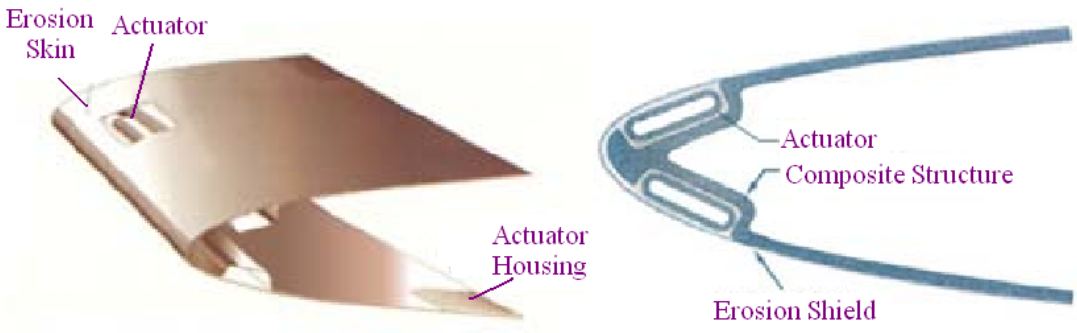

Figure 4-10 EMEDS Developed by Cox & Company

As an electromagnetic system, EMEDS has the similar advantages and limitations to EIDS. And the Cox electro-mechanical expulsive de-icing system is certified by FAA as a new ice protection technology, and has applications on Raytheon Premier I Horizontal Stabilizer and Raytheon Hawker Horizon Horizontal Stabilizer.

4.3 Thermal Ice Protection Systems

In modern aircraft, thermal ice protection systems are widely employed. They come in two main types: hot air and electro-thermal. Thermal ice protection systems provide heat to the protected surface continuously for anti-icing function or periodically to remove the accumulated ice. The heat is applied to the icing area, ensuring the surface temperature exceeds of freezing point, so that ice accretion is prohibited or the ice accumulation is removed. In recent years, a novel electro-thermal ice protection technology has been developed to minimize electrical power consumption, named pulse electro-thermal de-icing system. This system will be introduced in the following chapters.

4.3.1 Hot Air Anti-icing System

Hot air anti-icing system is the most common ice protection system applied on medium and large sized transport aircraft. Normally, engine bleed air is the hot air source, which is ducted to the leading edge to heat the icing surface. This system is often used on wings, empennages and nacelle lips. A typical hot air ant-icing icing system employed on engine nacelle lip is shown in Figure 4-11 [34].

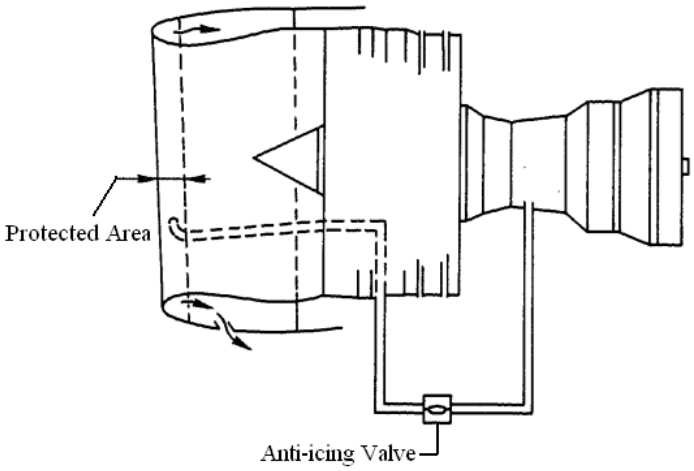

Figure 4-11 Nacelle Hot Air Anti-icing System

The system installation consists of ducts, a shutoff valve, a piccolo tube and other mechanical supports. The air bled from the fifth stage of the high pressure compressor is directed by the ducts to the piccolo tube which distributes hot air within the leading edge to heat the surface above freezing temperature. A solenoid-operated anti-icing valve provides on-off control.

Hot air anti-icing systems prohibit ice formation on the leading edges with no aerodynamic penalties. In addition, the system is simple and widely used, numerous references are helpful. Furthermore, as long as the engines function well, hot air is available for anti-icing. However, the biggest limitation is high level of power required for fully evaporated surfaces. Even operation in running wet conditions, the power consumption is quite considerable. The running wet conditions have another serious problem that water can run back to the unheated areas and the freezes. This runback ice accumulation could seriously impact the flight safety.

4.3.2 Electro-Thermal Ice Protection System

The principle of electro-thermal ice protection systems is to apply electrical energy on the protected area and heat the surface above freezing temperature, which protects against ice formation or melts existing ice accretion. This technology can be used on wing leading edges, empennages, nacelle lips, propellers, windshields and probes. For those areas where ice accumulation is not acceptable, such as nacelle lips, windshields and probes, electro-thermal anti-icing is employed. For other parts, where ice accumulation is not as serious, de-icing is accepted. A typical section of a heater is illustrated in Figure 4-12 [31]. The first layer is stainless steel, used as an erosion shield. The second and the forth ones are insulation to keep electricity in isolation. The heat element is shown with red color between insulations.

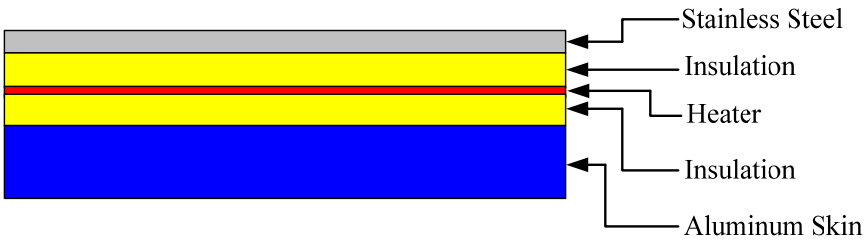

Figure 4-12 Typical Section of Electrical Heater

A typical example of electro-thermal anti-icing systems for windshield is shown in Figure 4-13 [34]. The system includes heat elements embedded in the windshield, temperature sensors and window heat computers. De-fogging system is also designed for the sliding windows and fixed windows. The temperature range of each window is controlled from 35 to 42 ℃. However, when the temperature is more than 60 ℃, the heat electricity is cut off to prevent overheat for the windows safety.

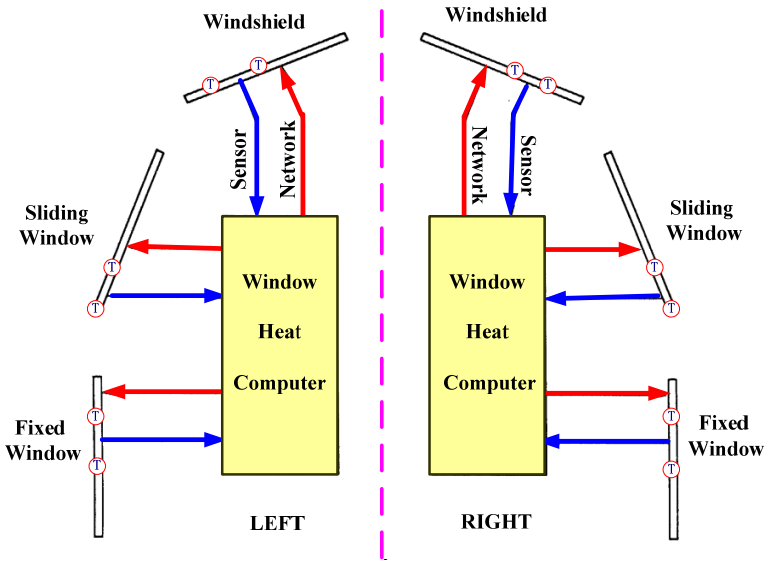

Figure 4-13 Window Heat System Schematic

When functioning as a de-icing tool, electrical power is applied on the icing surface interface to melt the bonding layer and then aerodynamic forces remove the ice bulk. The heaters are usually divided into parting strips and cycled shedding zones, see Figure 4-14 [31]. Parting strips may be distributed in spanwise and chordwise directions, which are used to segment the ice cap so that the aerodynamic force can

blow the ice bulk away easily. Parting strips operate in anti-icing mode. Cycled shedding zones are activated sequentially for power saving, which is a de-icing function to melt the ice bonding at the interface.

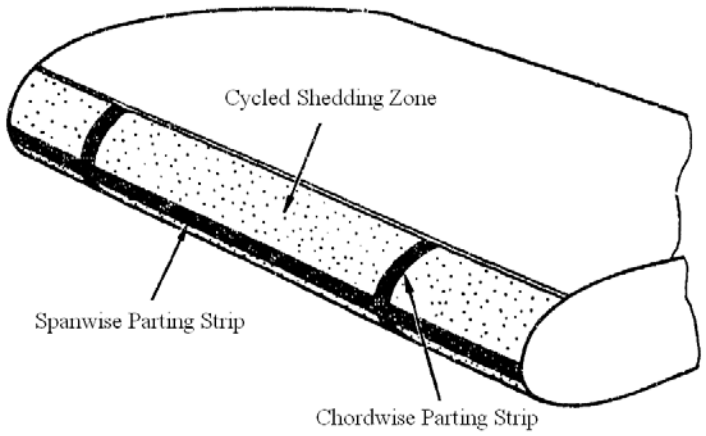

Figure 4-14 Parting Strips and Shedding Zone

Electro-thermal ice protection systems are efficient, and particularly suitable for windshields and probes. And the heat element can be easily to be tailored to fit the application. However, for larger areas that require ice protection, such as wings and empennages, electro-thermal anti-icing consumes too much energy. So it is more practical to adopt de-icing on these large parts. Even doing this, the required power is still in high level. Runback icing may occur on the unprotected surfaces in such systems, causing aerodynamics degradation.

4.3.3 Pulse Electro-Thermal De-icing System

As mentioned above, conventional Electro-Thermal De-icing Systems (ETDS) have two drawbacks, one is the high level of power consumption and the other is runback icing. In order to solve these problems, Pulse Electro-Thermal De-icing Systems (PETDS) have been developed and demonstrated by Goodrich [35,36].

PETDS employs an electro-thermal pulsing technique. The heating elements are also divided into parting strips and shedding zones. The parting strips are energized with

constant power density to keep the surface temperature above freezing. The shedding zones are energized periodically with short intense pulses of power to melt the interface of the ice on the surface of the leading edge. This short burst pulsing power can minimize the energy losses to the ambient. It was reported by Goodrich that this system consumes 20% to 50% less energy than that required for a conventional electro-thermal de-icing system with an average power density of less than 1.5 W/in^2 at -4 ℉.

The very high density power is energized to the protected surface as quickly as possible. This power only melts a very thin ice layer, so the possibility of melted runback water is minimized. Furthermore, the heaters are designed with low thermal mass located directly on the icing surface. So the air flow can cool the skin temperature below freezing very quickly when the power is cut off. So the impinged water freezes quickly resulting in minimal runback ice formation.

The PETDS was installed on a technology demonstrator airplane by Goodrich, see Figure 4-15. The PETDS consists of left outboard heaters (1 in Figure 4-15[35]), right outboard heaters (2), one electronic controller/monitoring unit (3), two energy storage units (4) and one cockpit control unit(5).

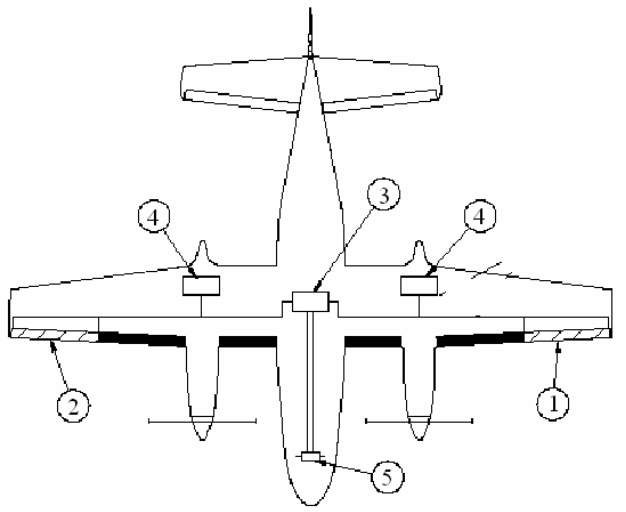

Figure 4-15 PETDS Generic Schematic on Goodrich Demonstrator

The heaters are installed at the outboard section of each wing, with spanwise extent of approximately 66". The parting strip is located beneath the leading edge skin around the stagnation line and the low thermal mass shedding zones are installed directly on the leading surface. The cross section of heater is illustrated in Figure 4-16[35].

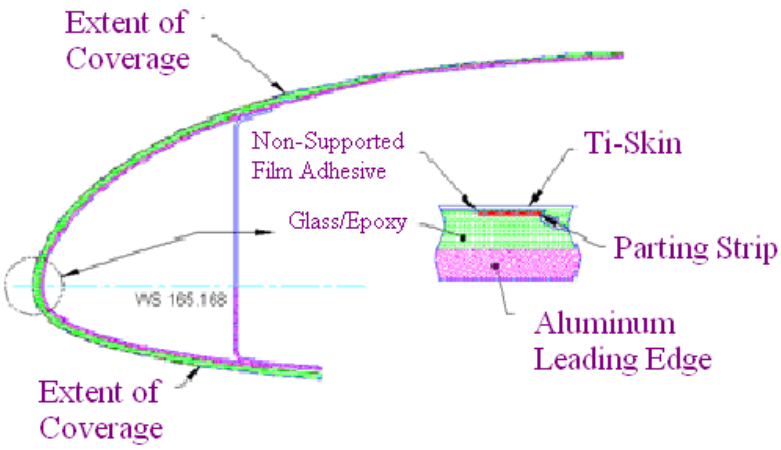

Figure 4-16 PETDS Heater Cross Section

An electronic controller monitors the temperature and parting strip heaters current as well as the charge voltage of the energy storage units. Once one of these parameters is excess of the limit, system fail indication is displayed. The energy storage units, installed in cargo bays located on the top of each wing in proximity to the engine nacelles, are used to supply pulse energy to the heaters. The cockpit control unit is installed on the copilot's instrument panel and used to be remote control of the system.

In conclusion, PETDS is a good solution to the inherent problems of conventional ETDS. However, because of the use of parting strips as running wet anti-icers, the required power level is still high. In addition, runback ice accumulation is minimized, but it does not mean the runback ice is completely avoided. The ice accumulation beyond the heating area still brings aerodynamics penalties and will last for long period until the ambient temperature is above freezing point or may even be the entire duration of the flight on a very cold day.

4.4 Hybrid Ice Protection Systems

A hybrid ice protection system has been developed by Cox & Company, Inc [37]. This hybrid system consists of a running wet electro-thermal anti-icing system and an EMEDS, see Figure 4-17[37]. The objective of this system was to develop an alternative to existing high power anti-icing systems on roughness-sensitive airfoils where high power is either impractical or unavailable. The electro-thermal running wet system keeps sensitive zones above freezing temperature, requiring less power because the surface temperature is just above freezing. The runback water freezes downstream where the EMEDS is installed to remove this ice accumulation periodically.

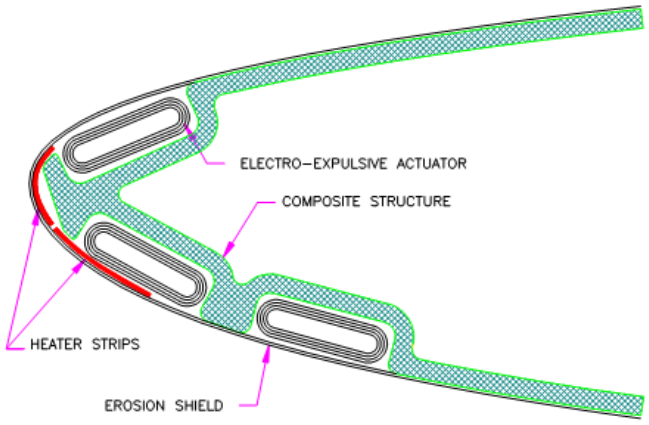

Figure 4-17 Schematic of Hybrid System Tested by NASA

This system has been tested in the NASA Lewis Icing Research Tunnel on a horizontal stabilizer section of a light business jet [37]. From the test, some valuable conclusions were reached:

a) The power required for the hybrid system is relatively small, only a fraction of that of evaporative systems, however it has little difference in overall performance. The power required for evaporative system is at least 570% greater than that consumed by the hybrid system.

b) Aircraft equipped with this hybrid system could operate in the icing conditions for indefinite periods. The reason is that all runback ice can be removed by the actuators in the EMEDS.
c) It is possible that this hybrid system is an effective solution to aircraft when flying in SLD icing conditions. EMEDS requires significantly lower power to operate, so it is feasible to extend the protected surfaces to a larger area which could cover the impinged zone stroke by SLD.

The solution of a hybrid running-wet anti-icing system concentrates on roughness-sensitive airfoils with lower required power. However, running wet hybrid configuration still needs considerable power for anti-icing on the roughness sensitive leading edges. Consequently, a new type of hybrid system has been developed to perform ice protection on icing surfaces at even lower power for roughness sensitive airfoils. This system is called Thermo-Mechanical Expulsion Deicing System (TMEDS) [1].

TMEDS combines EMEDS and PETDS together, see Figure 4-18[1]. Generally, the heater of PETDS covers the entire impinged zone or the stagnation region and the upper impinged surface. The actuators of EMEDS are mounted to chordwise ribs, covering from the leading edge to the runback ice zone. The heating by PETDS and flexing by EMEDS are applied on the protected skin in a coordinated fashion locally. PETDS is used to heat the interface between ice layer and skin and only a thin layer of ice is melted, so that the level of ice adhesion is reduced and thereby the bond at the surface is weakened. At this time, the heat power is switched off and the actuators are fired to flex the skin and remove the accumulated ice. Due to the ice layer bond is weakened before, the ice accretion can be shed completely and keep the roughness sensitive surfaces free of ice.

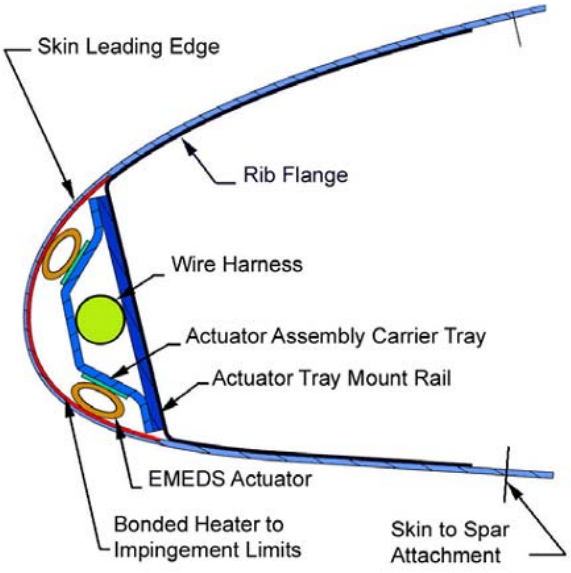

Figure 4-18 TMEDS Hybrid Deicing System Configuration

Unlike the hybrid running wet anti-icing system, PETDS in TMEDS eliminates the need for parting strips and adopts the electro-thermal pulsing technology. Therefore, TMEDS can operate with significantly lower power than the hybrid running wet anti-icing systems with electro-thermal de-icing. Because of using EMEDS in TMEDS, the runback ice buildup is easily to be removed, thereby allowing very long and unrestricted exposure to icing conditions. In addition, problems caused by SLD are solved.

4.5 Conclusions

An ice protection system with high efficiency and low power consumption is the perfect choice for engineering applications. From the different types of IPS discussed above, the characteristics of each system are summarized here.

Fluid ice protection system has little application due to the limitation of fluid supply and fluid weight, though the power required is minimal.

Mechanical de-icing systems require minimal energy, but the de-icing efficiency is not high enough. For example, pneumatic boot de-icing system may cause ice bridge

above the boot surface. Another concern is that EMEDS does not remove low levels of ice accumulation built around the stagnation line where thin ice forms at high temperature and high speed conditions. These problems are due to the fact that mechanical de-icing systems need sufficient a thickness of ice to be removed efficiently.

Thermal ice protection systems can operate as fully evaporative anti-icing, ensuring no ice accumulation on the leading surface with highest efficiency. However, the power required is too high and it is impractical for power unavailable aircraft. Even though it can be applied in running wet or de-icing modes, the power consumption is still too high. In addition, these operating modes can cause runback ice accumulation on the unprotected surfaces, which is detrimental to the aerodynamics performance.

In order to achieve the objective of high efficiency and low power consumption, a hybrid ice protection system has been developed, named TMEDS. It combines PETDS and EMEDS together, having several advantages over any single ice protection system:

a) The anti-icing parting strip is eliminated from the leading edge and pulsing electro-thermal de-icing technology is used, reducing power consumption.
b) Ice ridges, generated beyond the heaters, are prevented by actuators of EMEDS, allowing long time flight in icing environment without restrictions.
c) The bond of accumulated ice on the rough sensitive interface is weakened, so ice accretion is easily removed by EMEDS with high efficiency.

As has been seen, hybrid EMEDS achieves the objectives of high efficiency and low power consumption. It is one of the most promising systems for future application on aircraft. That is why the author chose this system as his research topic. In the next chapter, the system power calculation methods of each subsystem will be investigated, and the solution methodology and results will be also explained respectively.

5 Parameters Calculation of TMEDS

The primary parameters of TMEDS will be discussed in this chapter, including the calculation methodology. Due to the combination of PETDS and EMEDS, the discussion will focus on these subsystems respectively. In order to compare with conventional ETDS in term of power consumption, ETDS power consumption calculations will also be investigated.

5.1 Calculation Methodology

5.1.1 Pulse Electro-Thermal De-icing System

In order to minimize the power consumption of electro-thermal de-icing systems, pulsing technology is employed. The pulsing power operates on the icing surface instantaneously and melts only a very thin layer of interfacial ice, leaving the temperature of the environment untouched. Therefore, there is no heat loss to the ambient air and melting just a thin ice layer only requires a small amount of power.

To melt the interfacial ice more economically, a thin-film heater is installed directly on the interface, thus reducing the thermal resistance between ice and the heater. Furthermore, the extremely short heat on time can prevent heat exchange between the heater and the environment. The typical layout of this de-icing heater is shown in Figure 5-1[38].

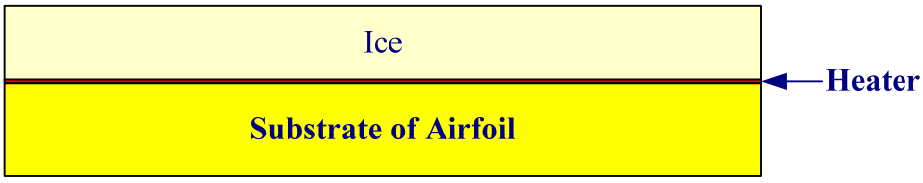

Figure 5-1 Typical De-icing Heater

The calculation methodology is introduced in Reference [38]. Within the pulsing time, the distance l of ice layer is given in the following equation.

$$l = \sqrt{\alpha_i \cdot t} \tag{1}$$

Where subscripts i refer to ice, is the thickness of ice formation on the icing surface, t is the pulsing time. α_i is the ice coefficient of heat diffusivity, giving by:

$$\alpha_i = \frac{\lambda_i}{\rho_i c_i} \tag{2}$$

Where λ_i is ice thermal conductivity coefficient, ρ_i is ice density and c_i is ice heat capacity.

The total energy required to melt a very thin layer of ice is:

$$Q = Q_m + Q_i + Q_h \tag{3}$$

Where Q_m is the energy to warm up the interfacial ice from original temperature to melting point, Q_i is the energy to melt he minimum thickness of ice layer and Q_h is the energy consumption to warm up the heater itself.

Q_m is given by:

$$Q_m = \frac{\pi(T_m - T_0)}{4P}\left[\sqrt{\lambda_i \rho_i c_i} + \sqrt{\lambda_s \rho_s c_s}\right]^2 \tag{4}$$

Where T_m is the ice melted temperature, T_0 is the original temperature, P is heating power, subscripts s refer to substrate of airfoil, λ_s is substrate thermal conductivity coefficient, ρ_s is substrate density and c_s is substrate heat capacity.

Q_i is given by:

$$Q_i = \rho_i d_i \gamma_i \tag{5}$$

Where d_i is melted ice layer thickness, and γ_i is ice latent heat of fusion.

Q_h is given by:

$$Q_h = C_h \rho_h d_h \tag{6}$$

Where subscripts h refer to heater, ρ_h is heater density, d_h is heater thickness, and C_h is heat capacity.

Thus the total energy required for melting the thin ice layer is summarized by:

$$Q = \frac{\pi(T_m - T_0)}{4P}\left[\sqrt{\lambda_i \rho_i c_i} + \sqrt{\lambda_s \rho_s c_s}\right]^2 + \rho_i d_i \gamma_i + C_h \rho_h d_h \tag{7}$$

In addition, the total energy can be also calculated by:

$$Q = P \cdot t \tag{8}$$

5.1.2 Electro-Magnetic Expulsion De-icing System

Electromagnetic force and power consumption are the primary parameters of electromagnetic expulsion de-icing systems.

For the coil, the electromagnetic force of each actuator is approximately given by [32]:

$$F = \frac{C_1 l N^2 I^2}{b}\left[\tan^{-1}\frac{b}{d_m} - \frac{d_m}{2b}\ln\frac{d_m^2 + b^2}{d_m^2}\right] \tag{9}$$

Where C_1 is a constant of 4×10^{-7}, l is the length of the coil, b is the width of the conductive strip, d_m is the mean space between the winding coil, I is the coil

current, and N is the number of coil winding turns. Some of these properties are shown in Figure 5-2[32].

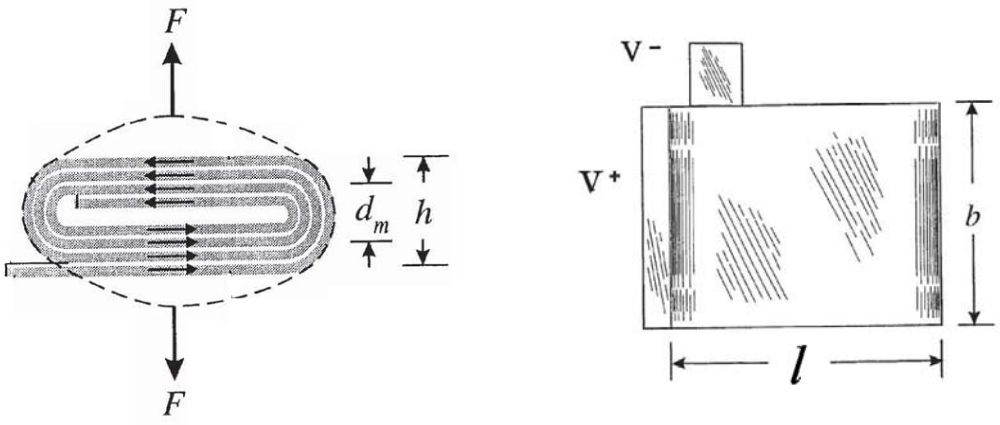

Figure 5-2 Properties of the Coil

Normally the circuit of EMEDS is a typical LRC circuit, as shown in Figure 5-3. When the switch S is connected to point a, the capacitor is charging from the electric source. When the de-icing signal is activated, switch S turns from a to c and discharges to cause an electromagnetic force in the actuator. In order to avoid circuit oscillation, overdamped response configuration is applied to ensure current decay.

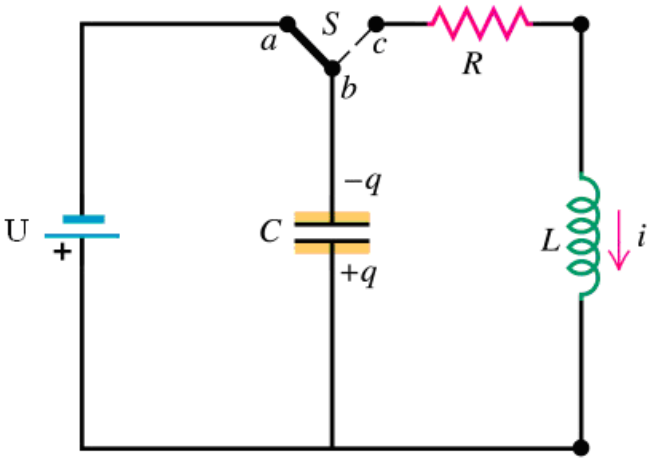

Figure 5-3 Typical LRC Circuit of EMEDS

The current $i(t)$ in the coil is given by [39]:

$$i(t) = A_1 e^{s_1 t} + A_2 e^{s_2 t} \tag{10}$$

Where s_1 and s_2 are given by:

$$s_{1,2} = -\frac{2R}{L} \pm \sqrt{(\frac{R}{2L})^2 - \frac{1}{LC}} \tag{11}$$

Where R is the resistance, C is the capacitance and L is coil inductance.

L is given by:

$$L = \frac{N^2 \mu_0 l d_m}{b} \tag{12}$$

Where μ_0 is the permeability of free space.

$u_c(t)$ is given by:

$$u_c = \frac{1}{C} \int_0^{t_0} i(t) dt \tag{13}$$

Where t_0 is the capacitor discharging time.

The power consumed by each actuator is determined by:

$$P = \frac{1}{t_0} \int_0^{t_0} u_c(t) \cdot i(t) dt \tag{14}$$

5.1.3 Electro-Thermal De-icing System

Electro-thermal de-icing system consists of parting strips and shedding zones. Due to the different functions, the power requirements for parting strip anti-icing and shedding zone de-icing is introduced respectively.

The various layers of a typical heater are illustrated in Figure 5-4[40]. The layers of different material are represented by the different colors. Besides the outer layer of ice, there are 6 layers adhesives to each other. The first layer is the erosion shield which is a kind of aluminum material. The second and the forth ones are elastomer used to keep electricity insulation. The heat element is shown with red color between the elastomers. The fifth dark blue colored layer represents the underlying structure and the silicon foam is used to minimize the heat loss to the slat inside.

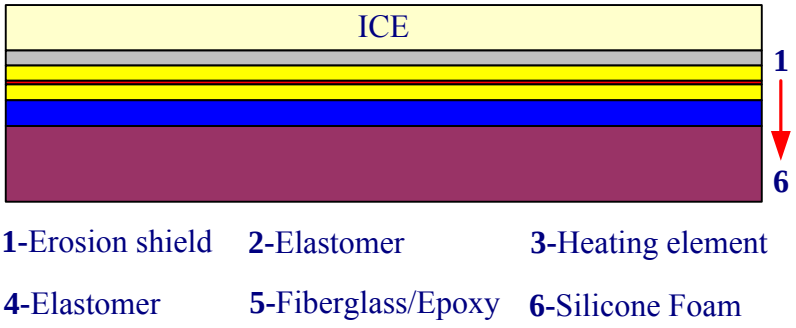

Figure 5-4 Layout of Different Layers

Parting Strip Anti-icing Power Consumption

Through the analysis of heat balance between the airfoil and airstream, the power consumption used to keep the leading surfaces above freezing point can be calculated. Reference [41] gives the calculation methods.

$$q = q_c + q_w + q_e - q_v - q_{ke} \tag{15}$$

Where q_c is heat loss due to convection, q_w is heat loss due to warming the impinged water, q_e is heat loss due to evaporation, q_v is heat gain due to viscosity and q_{ke} is heat gain due to kinetic energy of the water droplets.

Heat loss due to convection is given by:

$$q_c = h_c(T_s - T_0) \tag{16}$$

Where h_c is the convective coefficient, T_s is the temperature of skin surface and T_0 is the ambient temperature.

h_c is given by

$$h_c = 1.74 \times 10^{-2} \frac{(P_0 \cdot V_0)^{0.5}}{D} \tag{17}$$

Where P_0 is the ambient pressure, V_0 is the flight speed, and D is the equivalent leading edge diameter, normally it is calculated by 30% of the maximum thickness of the airfoil.

Heat loss due to warming the impinged water is given by:

$$q_w = m_w \cdot c_{p,w}(T_s - T_0) \tag{18}$$

Where m_w is the amount of impinged water, and $c_{p,w}$ is the water specific heat capacity with constant pressure.

Heat loss due to evaporation is given by:

$$q_e = m_e \cdot \gamma_e \tag{19}$$

Where m_e is the amount of evaporated water, and γ_e is the water latent heat of evaporation.

m_e is given by:

$$m_e = \frac{0.7 h_c}{c_{p,a} \cdot P_0} \left(P_{sat,s} - P_{sat,0} \right) \tag{20}$$

Where $c_{p,a}$ is the air specific capacity at constant pressure, $P_{sat,0}$ is the water saturated vapor pressure at ambient temperature, and $P_{sat,s}$ is the saturated vapor pressure at surface temperature.

Heat gain due to viscosity is given by:

$$q_v = h_c \cdot R_c\left(\frac{V_0^2}{2c_{p,a}}\right) \tag{21}$$

Where R_c is the recovery factor.

Heat gain due to kinetic energy of the water droplets is given by:

$$q_{ke} = \frac{m_w \cdot V_0^2}{2} \tag{22}$$

Summarizing formularies from (15) to (22), the total power need for parting strip anti-icing is calculated by:

$$q = m_w\left[c_{p,w}(T_s - T_0) - \frac{V_0^2}{2}\right] + h_c\left[(T_s - T_0) + \frac{0.7\gamma_e}{c_{p,a} \cdot P_0}(P_{sat,s} - P_{sat,0}) - \frac{R_c \cdot V_0^2}{2c_{p,a}}\right] \tag{23}$$

Shedding Zone De-icing Power Consumption

Shedding zones operates as a de-icing function, and the temperature diffuses from the heater to the external skin surface to melt a layer ice. Normally, the skin dimension along the chorwise and spanwise is much longer than the thickness, so a one-dimension model is employed to calculate the de-icing power.

For constant layer properties, perfect thermal contact between layers and one-dimension unsteady heat conduction, the mathematical models follow as [42]:

$$\rho_j c_j \frac{\partial T_j}{\partial t} = \lambda_j \frac{\partial^2 T_j}{\partial x^2} + q_j \tag{24}$$

Where subscripts j refer to different layers shown in Figure 5-3. For $j = 1,2,4,5,6$, $q_j = 0$, for $j = 3$, $q_j = \text{constant}$.

For the ice layer, the mathematical model is:

$$\frac{\partial H_i}{\partial t} = \frac{\partial}{\partial x}\left(k_i \frac{\partial T_i}{\partial x} \right) \tag{25}$$

Where subscripts i refer to ice layer, H_i is the enthalpy, T_i is the temperature and k_i is the thermal conductivity.

H_i is given as follows:

$$H_i = \begin{cases} \rho_S c_S T_i & T_i < T_m \\ \rho_L c_L (T_i - T_m) + \rho_L (c_S T_m + \gamma) & T_i > T_m \end{cases} \tag{26}$$

Where the subscripts S and L refer to solid and liquid phase respectively, T_m is the melted temperature and γ is the latent heat of fusion.

The temperature and heat fluxes are continuous at the layer interfaces and the boundary conditions at the layer interfaces are given by:

$$\begin{aligned} & T_j\big|_I = T_{j+1}\big|_I \\ & k_j \frac{\partial T_j}{\partial x}\bigg|_I = k_{j+1} \frac{\partial T_{j+1}}{\partial x}\bigg|_I \end{aligned} \qquad j = 1,\cdots,5 \tag{27}$$

Where subscripts I refer to interface.

The boundary condition at the exterior surface is given by:

$$k_1 \frac{\partial T_1}{\partial x}\bigg|_{\mathrm{EXT}} = h_{\mathrm{EXT}}(T_1|_{\mathrm{EXT}} - T_{0,\mathrm{EXT}}) \tag{28}$$

Where subscripts EXT refer to exterior surface, h_{EXT} is heat transfer coefficient and $T_{0,\mathrm{EXT}}$ is the ambient temperature of exterior surface.

The boundary condition at the interior surface is given by:

$$k_6 \frac{\partial T_6}{\partial x}\bigg|_{\mathrm{INT}} = h_{\mathrm{INT}}(T_6|_{\mathrm{INT}} - T_{0,\mathrm{INT}}) \tag{29}$$

Where subscripts INT refer to interior surface, h_{INT} is heat transfer coefficient and T_{INT} is the ambient temperature of interior surface.

The initial condition is presented by:

$$T_j = T_0 \qquad j = 1,\cdots,6 \tag{30}$$

5.2 Calculation Results and Analysis

5.2.1 Pulse Electro-Thermal De-icing System

Pulsing time should be less than the time it takes heat to diffuse in the ice layer so that heat losses to the ambient air are neglected. From formulas (1) and (2), we can derive the longest time. Based on the given pulsing time, power consumption and energy cost can be calculated through formulas (7) and (8). Before calculating, the required material properties are listed in Table 5-1[40].

Table 5-1 Material Properties of Pulse Electro-Thermal De-icing System

Material	λ (W/mK)	ρ (kg/m^3)	c (J/kg℃)	d (mm)
Ice	2.2	920	1960	1.27

Heater (Ti-6Al-4V[43])	16.3	8025	502	0.2
Substrate (Elastomer)	0.256	1384	1256	0.45

The maximum pulsing time $t_{max} = 1.3$ s. In addition, the power consumed by heater, melting ice and warming ice and substrate is summarized in Table 5-2.

Table 5-2 Power Consumption by Different Material

Total Power, P	46.4 kW	100%
Power by heating heater , P1	9.1 kW	19.6
Power by melting ice , P2	0.5 kW	1.1%
Power by warming ice and substrate , P3	79.3 kW	79.3%

From Table 5-2, it can be seen that power used to warm ice and substrate account for nearly 80% of the total power, which is the largest proportion. Moreover, power consumed by the heating heater itself takes 19.6% and power used to melt the accumulated ice is only 1.1%. However, this small quantity of power is very significant because melting a thin layer of ice is the chief objective of PETDS.

The power and energy consumption against different pulsing times are illustrated in Table 5-3 and Figure 5-5.

Table 5-3 Power Consumption versus Pulsing Time

t/s	0.1	0.3	0.5	0.7	0.9	1.1	1.3
P/kW	223.8	109.3	80.3	65.9	57.1	51.0	46.4
Q/kJ	22.4	32.8	40.1	46.1	51.4	56.0	60.3

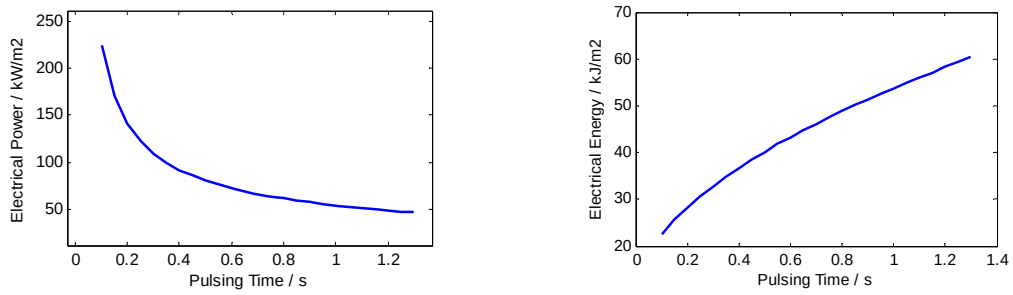

Figure 5-5 Power and Energy Consumption versus Pulsing Time

From these calculation results, it is clear that power consumption falls quickly with the increase of pulsing time while the energy goes up. So a trade off analysis is needed to decide which pulsing time is the most optimum choice.

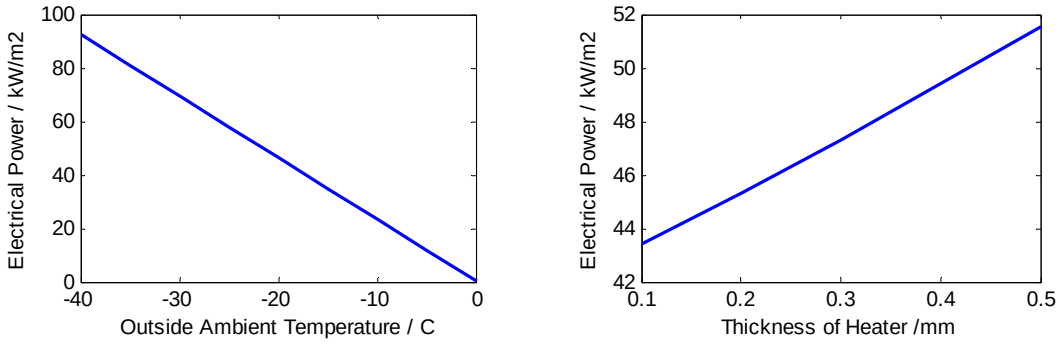

(a) (b)

Figure 5-6 Power Consumption versus OAT and Heater Thickness

According to Figure 5-6(a), it is clear that power consumption decreases significantly when Outside Air Temperature (OAT) goes up from -40 to 0 ℃. The reason is that at lower temperatures more power is required to warm the ice layer, heater and substrate up to the melting point. Also as shown in Figure 5-6(b), the electrical power rises with increase in heater thickness. A thicker heater means higher thermal capacity, so more power is applied to heat the heater itself.

5.2.2 Electro-Magnetic Expulsion De-icing System

In the calculation conditions in Table 5-4 [32], the power consumption is nearly 380

kW and causes an electromagnetic force of 177.1 Newtons.

Table 5-4 Calculation Parameters of EMEDS

Coil Properties				Electrical Parameters				Calculation Results	
N	l/m	b/m	d_m/m	U/V	L/mH	R/Ω	C/μF	P/kW	F/N
75	0.019	0.019	0.0025	550	179.4	0.55	250	379.8	177.1

The power consumption and electromagnetic force versus coil turns are illustrated in Figure 5-7. With the increase of turns of coil, the electrical power and electromagnetic force decrease.

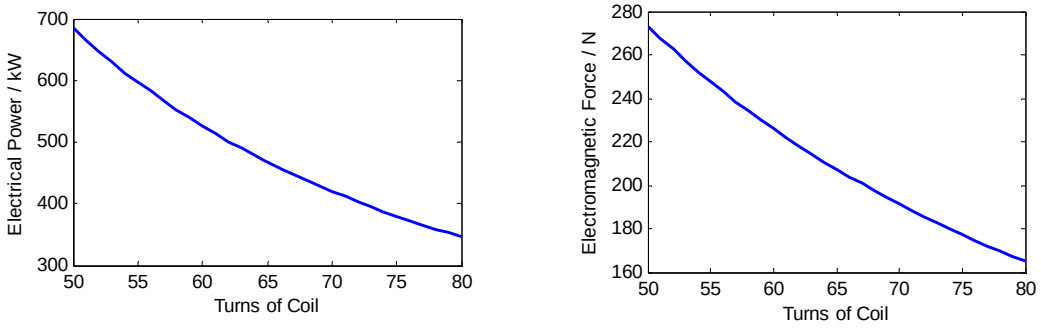

Figure 5-7 Power Consumption and Electromagnetic Force versus Coil Turns

The power consumption and electromagnetic force versus voltage are shown in Figure 5-8. The electrical power and electromagnetic force rise with the increase of voltage.

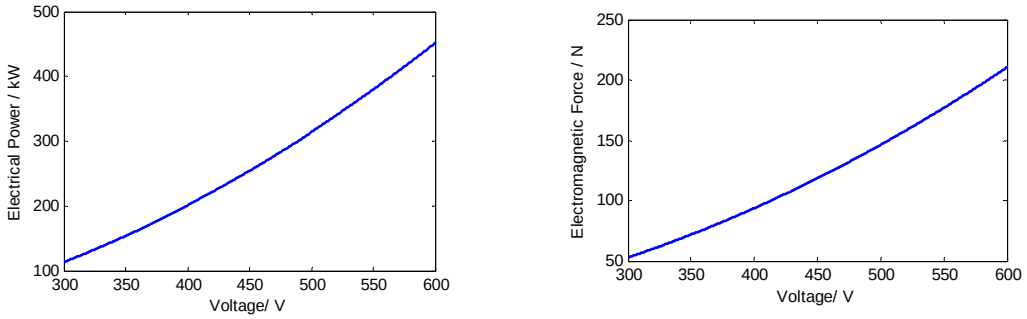

Figure 5-8 Power Consumption and Electromagnetic Force versus Voltage

5.2.3 Electro-Thermal De-icing System

As to Figure 5-4, the material properties of different layers are shown in Table 5-5 [40].

Table 5-5 Layer Material Properties

Layer	Material	λ (W/mK)	ρ (kg/m^3)	c (W/kg℃)	δ (mm)
	Ice	2.2	920	1960	1.27
1	Erosion shield	16.3	8025	502	0.2
2	Elastomer	0.256	1384	1256	0.28
3	Heating element	41.0	8906	385	0.013
4	Elastomer	0.256	1384	1256	0.28
5	Fiberglass/Epoxy	0.294	1794	1570	0.89
6	Silicone Foam	0.121	642	1130	3.43

The flight calculation conditions and icing calculation conditions are listed in Table 5-6 [6, 48].

Table 5-6 Flight Calculation and Icing Calculation Conditions

V_0 /(m/s)	P_0 (Pa)	T_0 /℃	LWC /(g/m^3)	MVD / μm
160	54000	-10	0.3	25

The calculation results of different parts of power consumption for parting strips are given in Table 5-7. From this table, we can see that heat loss due to evaporating the liquid water takes the biggest percentage. The second one is the power used in convection and the smallest portion is the heat gain due to kinetic energy of the water droplets. In these calculation conditions, the energy generated by viscosity contributes a lot to heat the leading edge.

Table 5-7 Layer Material Properties

	q	q_c	q_w	q_e	q_v	q_{ke}
Power/kW	14.8	11.8	1.2	13.3	-11.1	-0.3
Percentage/%	100	79.7	8.1	89.9	-75.0	-0.02

The power consumption versus flight speed and OAT are show in Figure 5-9. From Figure 5-9 (a), it can be seen that power consumption goes up as the flight speed is less than approximate 115 m/s. After 115 m/s, the power consumption decreases sharply. The underlying reason for this phenomenon is as flight speed increases a greater proportion of power is consumed by heat due to viscosity. In Figure 5-9 (b), more power consumption is required at lower temperature, because a considerable energy is used to heat colder air and structure at lower temperature conditions.

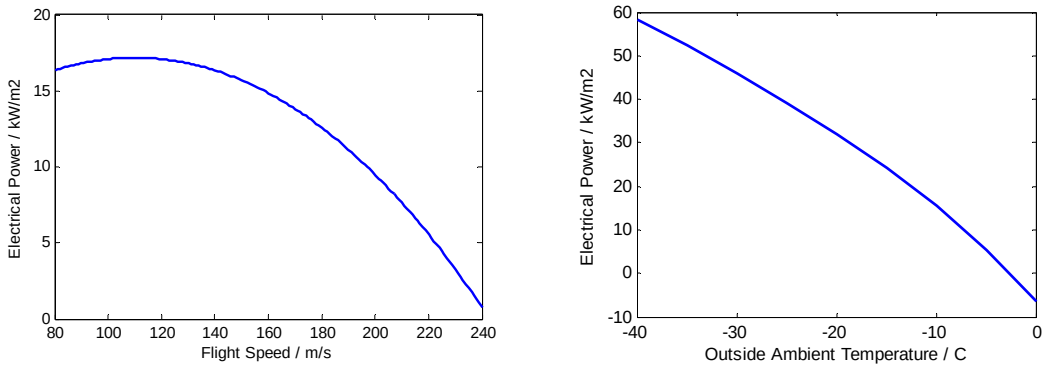

(a) (b)

Figure 5-9 Power Consumption versus Flight Speed and OAT

For shedding zones, partial differential Equations (24), implicit finite difference methods can be used to solve these problems [44]. These explicit methods consider transient, one-dimensional conduction with constant properties. The second derivative with respect to the spatial coordinate can be expressed by a central difference approximation and the time derivative can be expressed as a forward difference approximation. Therefore, using the finite difference approximation, the solutions to

Equations (24) can be obtained respectively as

$$\frac{T_i^{n+1} - T_i^n}{\Delta t} = \alpha \frac{T_{i+1}^{n+1} - 2T_i^{n+1} + T_{i-1}^{n+1}}{(\Delta x)^2} + \frac{q_j}{\rho c} \tag{31}$$

Where subscript i indicates a spatial increment, superscript n denotes time interval, and α is the heat diffusivity coefficient.

As to layer interface and boundary conditions, the first derivative with respect to spatial coordinate $\partial T / \partial x$ is expressed by a forward difference approximation, given by:

$$k_j \frac{\Delta T_j}{\Delta x}\bigg|_I = k_{j+1} \frac{\Delta T_{j+1}}{\Delta x}\bigg|_I \qquad j = 1, \cdots, 5 \tag{32}$$

$$k \frac{\Delta T}{\Delta x}\bigg|_I = h_a (T\big|_I - T_a) \tag{33}$$

For partial differential equation (25), the Method of Assumed States (MOAS) is employed [45]. MOAS eliminates the need to solve enthalpy equation. Instead, the latent heat of the ice-water phase change is replaced by a very large heat capacity assigned over a very small temperature range.

In the calculation conditions shown in Table 5-6, with the heat-on time of 20 seconds, cycle time of 60 seconds and heat power of 6.2 kW, the skin surface temperature versus heat time is shown in Figure 5-10. At every end of heat-on time, the surface temperature can reach more than freezing point and the ice at interface between ice and skin is melted, so accumulated ice can be removed by aerodynamics forces. During the heat-off period, the skin surface is cooled down by the air stream and surface icing.

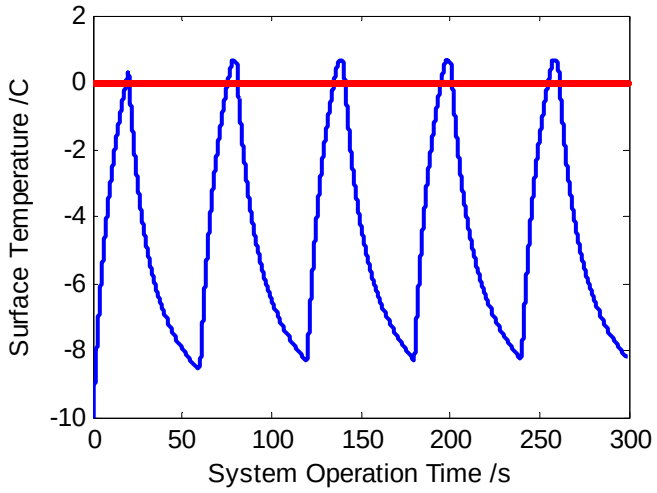

Figure 5-10 Surface Temperature versus Heat Time

The heat-on time is significant to heat power and runback water, thus it is necessary to study the parameters effects on heat-on time. From Figure 5-11, it can be seen that heat-on time decreases as heat power increases and as the heat-on time rises, the energy consumption increases. Therefore, when determining the system heat-on time and heat power, we need a trade-off discussion. On one hand, less heat-on time is needed to lower the amount of runback ice formation and energy consumption. On the other hand, less time requires a higher level of heat power. Therefore, under the allowed power supply requirements, high heat power level is expected.

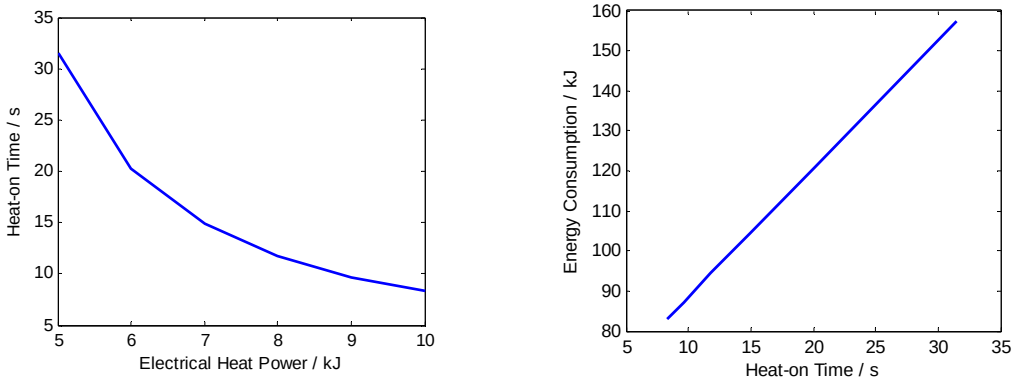

(a) (b)

Figure 5-11 Heat-on versus Electrical Power

Heat-on time increases significantly as OAT decreases, as shown in Figure 5-12. Lower ambient temperature requires more heating time to reach the ice melting point. However, as discussed above, longer heat-on time results in higher energy consumption and more runback water. An effective way to solve this problem is to increase heating power or adopt PETDS. When designing this system, the influence of ambient temperature on heat-on time should be considered and measures taken to ensure de-icing function.

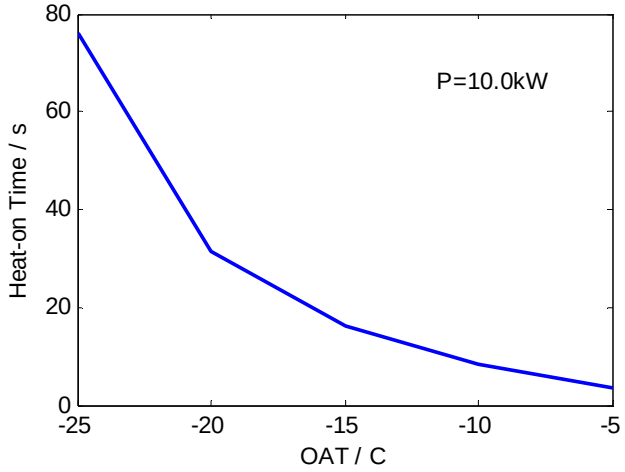

Figure 5-12 Heat-on Time versus OAT

5.3 Validation Considerations

The calculation mathematical models discussed above should be validated in order to explain the calculation accuracy. Two methods can be employed to conduct the validation, which are icing wind tunnel test and natural icing flight test. However, the cost of these methods is quite high and it is not practical in this one year MSc study. If there are no limitations on time and cost in the future research work, validation in icing wind tunnel test is feasible in Cranfield University.

Cranfield University is equipped with an ambient pressure icing tunnel at mixed industrial applications, research project work and teaching [46]. Some features of icing wind tunnel in Cranfield University are listed in Table 5-8 [47]. Based on these features,

the concerns about icing wind tunnel test are given below.

a) It is necessary to discuss all test issues with icing wind tunnel staffs, including test cost, test schedule arrangement, model installation, and other detailed issues.
b) Calculation and validation should maintain consistency with the same flight conditions and icing environment. These conditions must be in the range of Cranfield University icing tunnel capabilities.
c) Test model should not be too large in order to avoid tunnel blockage. The size of test model must be determined according to the test section dimensions.
d) The significant parameters should be recorded, including: test conditions, heating surface temperature, skin deformation (stress), ice shapes, applied voltage and current.
e) TMEDS should be demonstrated at different flight and icing conditions to illustrate effects of flight and icing conditions on de-icing efficiency and power consumption.
f) 45-minute icing with system switch on should be tested to evaluate icing effects on aerodynamic. This test can account for longtime flight in icing conditions without restrictions when equipped with TMEDS.

Table 5-8 Features of Cranfield University Icing Tunnel

Air Flow	Flow Rate	100 kg/sec
	Mach Number	0.1 ~ 0.5
	Total Air Temperature	- 30~30 ℃
Water Droplet	Droplet Sizes	15~80 microns
	Liquid water Content	0.05 to 3 g/m^3
Refrigeration and Heating	Cooling Capacity	500 kW
	Hot Air Sources	150 kW
Test Sections	760 x 760 mm, 810 mm octagonal & 400×400	

5.4 Discussion and Conclusions

In this chapter, power calculation methods of PETDS and ETDS are created based on one-dimension heat conduction model. The difference between PETDS and ETDS is that pulsing power is applied on the surface instantaneously during a short period in PETDS, leaving environment temperature untouched. Therefore, there is no heat convection in PETDS. Three concerns in the calculation models need to be discussed:

a) One-dimension model. This one-dimension model can ensure system basic performance and calculation accuracy because the thickness of heating layers is much less than the length in chordwise and spanwise. In order to get more accurate calculation results, 3-D model should be developed.
b) Constant material properties. The material properties of different heating layers are a function of temperature and this correlation was not considered in the calculation models. In fact, the properties change little during a narrow temperature arrange, so it has slight effects on calculation results. If highly accuracy is demanded, the variable properties corresponding to temperature should be added into the mathematical models.
c) Critical ice thickness. Because of time limitation, the critical ice thickness used to calculate power was obtained from Reference [1]. In order to get a more accurate critical ice shape, icing wind tunnel tests and icing effects on aerodynamics should be conducted.

The power calculation model of EMEDS is a typical LRC circuit with overdamped response configuration. Once the capacitance and applied voltage are determined, the energy consumed by EMEDS can be calculated easily. Thus the actual power depends on the EMEDS pulsing time. However, the power consumption during a de-icing cycled period of time is a practical mean to evaluate the system performance. Instead of pulsing time, a de-icing period is employed in power calculation. Therefore this LRC circuit model can satisfy the calculation requirements of this research.

The calculation results are summarized by:

a) Most power of PETDS is used to warm the ice and substrate and heat the heater itself in order to achieve the goal of melting a thin layer of ice. PETDS power consumption falls quickly with pulsing time increase. And power decreases significantly when OAT goes up and it rises with increase of heater thickness.

These results tell PETDS system designers that material with small thermal capacity is required for skin and heater to reduce power consumption. And this material selection should be under meeting other design requirements. Moreover, OAT has significant effects on system performance, so system heat control strategy should be designed according to OAT.

b) More coil turns and lower voltage can raise lower electrical power and electromagnetic force in EMEDS.

It is desirable to choose reasonable parameters and properties for satisfied electromagnetic so that ice accretion can be removed. However, this may need more power. Thus designers should optimize the system parameters with the goals of adequate force and acceptable power.

c) For ETDS, higher flight speed results in more viscosity heat to the leading edge and it is helpful to reduce parting strip power consumption. In addition, considerable energy is used to heat colder air and structure at lower temperature conditions.

These conclusions show that power applied on parting strips should be designed as a function of flight speed and OAT. At low speed and cold temperature, anti-icing function of parting strips should be achieved by high power levels. And also for flight with high speed and warm temperature, power consumption can be minimized.

d) Heat-on time of cycled shedding zones in ETDS decreases with the rise of heat

It is obvious that improving the power applied on cycled shedding zones is an effective way to reduce heat-on time. Heat-on time reduction can minimize runback ice and economize electrical energy. But heat-on time should not be too short due to power supply limitations.

6 Thermo-Mechanical Expulsion De-icing System

TMEDS system design is based on a civil aircraft named Flying Crane [48]. Flying Crane, orientating at China's domestic air market in 2020, is designed as a next generation airliner. It is a medium to short haul, single-aisle, 128-seat jet liner with a conventional configuration. In this chapter, the work focuses on TMEDS architecture design and then calculates system power consumption. Also, a comparison between TMEDS and ETDS is employed to explain the advantages and challenges of TMEDS.

6.1 System Architecture

Flying Crane has 5 slats, 3 of which need ice protection. Each slat is about 2674 mm long, and each actuator measures about 381 mm [1], so each slat is segmented into 7 de-icing zones. Each de-icing zone is protected with two actuators beneath the upper surface, one actuator inside the leading area and one actuator in the lower surface. On the leading area, heaters are installed to melt a thin layer of ice to improve the de-icing efficiency for ice sensitive area. The system schematic is shown in Figure 6-1.

The system consists of one De-icing Control Unit (DCU), 2 Energy Storage Banks (ESB) and 6 de-icing slats. The DCU has two functions, the first one is to supply high voltage to charge the capacitors within the ESB, and the other one is to provide control laws for capacitors to charge and discharge. The ESB is used to power actuators and heaters according to the control law. The DCU can be located beneath the cabin floor near the central wing box and the ESB can be installed centrally at the front spar in the fixed leading edge behind slat 3. These installations can limit the length of power cables to each slat, so the weight reduction is achieved, as well as resistive losses through electrical cables.

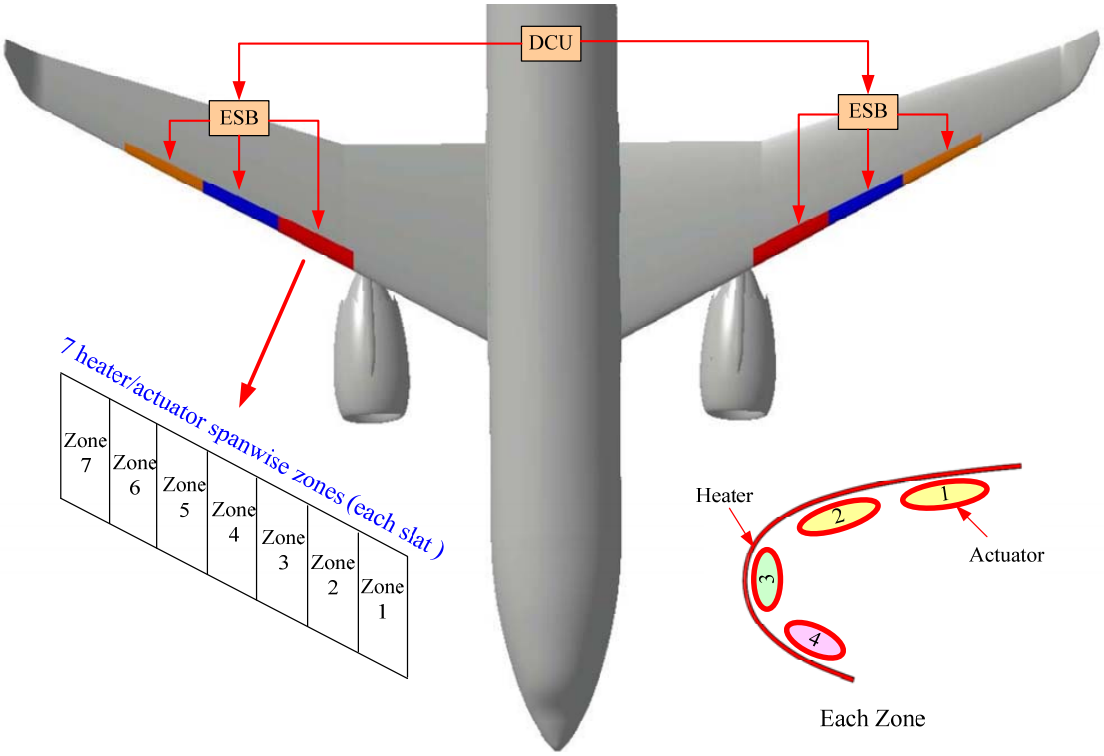

Figure 6-1 Thermo-Mechanical Expulsion De-icing System Schematic

The system is activated manually by flight crews when icing condition is detected. Two ESBs are discharged and energy is delivered through heaters and actuators to remove the ice accretion. The de-icing sequence is shown in Table 6-1.

Table 6-1 TMEDS De-icing Control Schematic

Slat	0~60s							
	0~4.3	4.3~8.6	8.6~12.9	12.9~17.2	17.2~21.5	21.5~25.8	25.8~30.1	30.1~60
2	Zone 1	Zone 2	Zone 3	Zone 4	Zone 5	Zone 6	Zone 7	
3	Zone 1	Zone 2	Zone 3	Zone 4	Zone 5	Zone 6	Zone 7	
4	Zone 1	Zone 2	Zone 3	Zone 4	Zone 5	Zone 6	Zone 7	

The cycle time is 60s and each zone is energized for 4.3 seconds. In the first 4.3 seconds, zone 1 of slats 2, 3, 4 are powered simultaneously, and then another 4.3 seconds for zone 2 of each slat until all the zones are powered during 30.1 seconds. From 30.1 to 60 seconds, no power is discharged and the ice will continue forming on

each zone to reach a reasonable thickness for higher de-icing efficiency. During each 4.3 seconds of each zone, the de-icing sequence is shown in Table 6-2.

Table 6-2 De-icing Zone Operating Sequence

Heater	Actuator 3	Actuator 1, 2, 4
0~1.3s	1.3~2.8s	2.8~4.3s

The heater is powered for 1.3 seconds to heat the surface, and then a thin ice layer at the interface is melted. After that, the corresponding actuator 3 behind the aerodynamic sensitive area is fired sequentially to remove the accumulated ice in 1.5 seconds. In the final 1.5 seconds, actuators 1, 2, 4 are activated simultaneously to break the ice accretion beyond the heater. Each actuator is fired typically 3 times per cycle in 4.3 seconds.

6.2 System Power Consumption

The power consumption is calculated based on one cycle time, 60 seconds. Power is consumed on heating icing surfaces and activating actuators, which will be discussed respectively.

For the PETDS, the maximum ice thickness is 1.3 mm [1], and in order to leave the temperature of the environment untouched, the pulsing time should be limited to 1.3 seconds. Here a maximum of 1.3 seconds are used as the pulsing time to minimize the pulsing power as discussed in 5.2.1. The power consumption calculation result is 23.3 kW/m^2 within the pulsing period of 1.3 seconds. The power and energy consumption used for heating each zone is shown in Table 6-3.

Table 6-3 Power and Energy Consumption for Heating

Slats/Zones		Area (m^2)	Power (kW)	Energy (kJ)
Slat 2	Zone 1	0.0640	1.49	1.94
	Zone 2	0.0628	1.46	1.90
	Zone 3	0.0615	1.43	1.86
	Zone 4	0.0603	1.40	1.83
	Zone 5	0.0590	1.37	1.79
	Zone 6	0.0578	1.35	1.75
	Zone 7	0.0565	1.32	1.71
Slat 3	Zone 1	0.0553	1.29	1.68
	Zone 2	0.0540	1.26	1.64
	Zone 3	0.0528	1.23	1.60
	Zone 4	0.0515	1.20	1.56
	Zone 5	0.0503	1.17	1.52
	Zone 6	0.0490	1.15	1.48
	Zone 7	0.0478	1.11	1.45
Slat 4	Zone 1	0.0465	1.08	1.41
	Zone 2	0.0453	1.06	1.37
	Zone 3	0.0440	1.03	1.33
	Zone 4	0.0428	1.00	1.30
	Zone 5	0.0415	0.967	1.26
	Zone 6	0.0403	0.939	1.22
	Zone 7	0.0390	0.909	1.18

Therefore during one de-icing cycle, the total energy consumption is 32.78kJ, with respect to 0.546 kW per cycle time 60 seconds (32.78/60=0.546kW).

For the EMEDS, the energy consumption is determined by voltage and capacitance of the ESB. The energy discharging from the capacitor can be calculated by $Q = \frac{1}{2}CU^2$.

It means that once the voltage U and capacitance C is confirmed, the energy consumption of actuators of EMEDS remains the same. Thus the power, discharging time, and electromagnetic force mainly depend on the properties of coils and the average power during one cycle period can be easily calculated.

It was reported that the capacitor with capacitance of 250~300μF is charged to 500~550 volts [1, 32]. Then the energy consumption ranges from 31.3 to 45.4 Joules. Here we take the maximum value 45.4 Joules as the design point for conservation design. Therefore in a one minute cycle period, the average power consumption of one actuator is 45.4/60=0.76 W, and for all the actuators, the power is 0.76×7×3= 16W = 0.016 kW. So the total power consumption for the whole TMEDS during one cycle period is 0.016+0.546=0.562 kW and the energy consumption is 0.562× 60=33.7 kJ.

6.3 Comparison with Electro-Thermal De-icing System

In order to make a comparison between TMEDS and ETDS, an ETDS system architecture is also built for Flying Crane. The system schematic is illustrated in Figure 6-2. The system mainly consists of one Wing Heat Controller (WHC), two Power Control Units (PCU) and 6 heaters. The system is designed to be activated manually, and once receiving activated signal from flight crews, WHC transmits switch on message to the PCUs. Then the PCUs turn on the electrical circuit to supply heating power to the heaters.

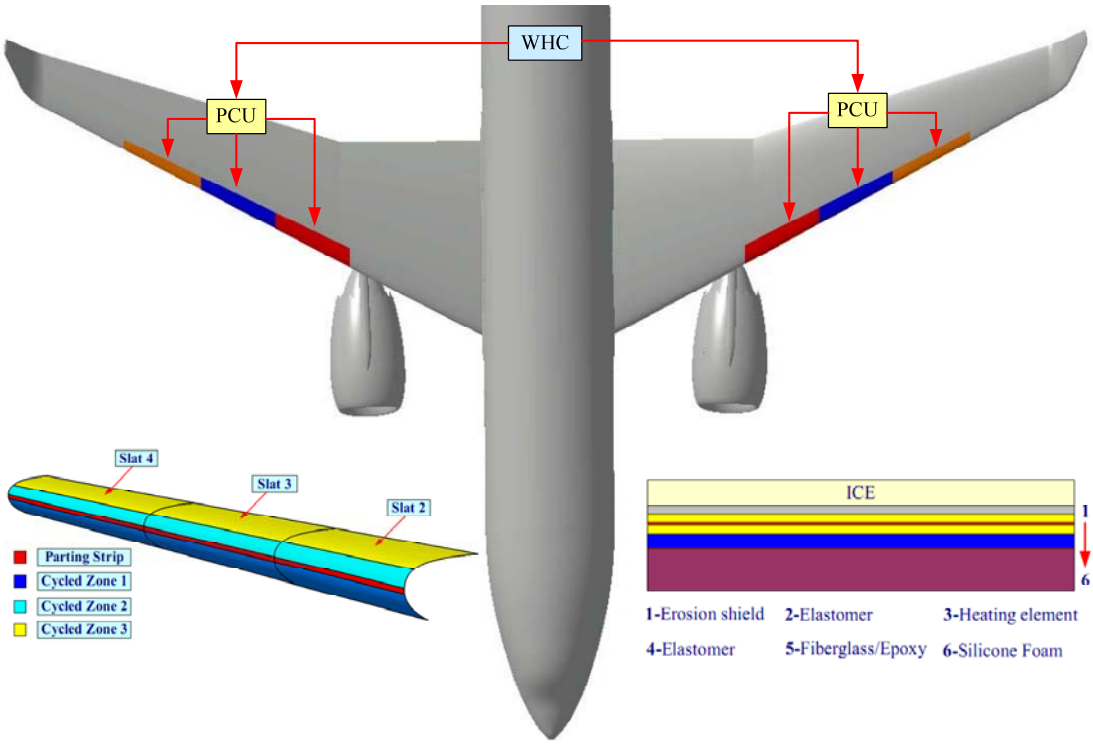

Figure 6-2 Electro-Thermal De-icing System Schematic

The system control law is shown in Table 6-4. The parting strip works through the entire cycle period. The heating on shedding zones of each slat lasts for 20 seconds and each shedding zone operate sequentially. So for each shedding zone, the heat-on time is 20 seconds and heat-off time is 40 seconds.

Table 6-4 Electro-Thermal De-icing Control Schematic

Heaters	0~60s		
	0~20	20~40s	40~60s
Slats 2, 3,4, Parting Strip			
Slat 2, Shedding Zone			
Slat 3, Shedding Zone			
Slat 4, Shedding Zone			

Through the calculation methods discussed in Chapter 5.2.3, the power and energy requirements for ETDS of Flying Crane are listed in Table 6-5. The total energy consumed in a cycle is 777.4kJ, and the power with respect to one minute is

777.4kJ/60=13.0kW.

Table 6-5 Electro-Thermal De-icing Power and Energy Consumption

Heating Zones		Power (kW/m^2)	Area (m^2)	Total Power (kW)	Total Energy (kJ)
Heaters, Slat 2	Parting Strip	13.0	1.17	1.17	70.2
	Cycled Zone 1	4.6	3.01	3.01	60.2
	Cycled Zone 2	5.2	1.77	1.77	35.4
	Cycled Zone 3	5.0	6.29	6.29	125.8
Heaters, Slat 3	Parting Strip	14.1	1.13	1.13	67.8
	Cycled Zone 1	4.6	2.64	2.64	52.8
	Cycled Zone 2	5.3	1.51	1.51	30.2
	Cycled Zone 3	5.1	5.32	5.32	106.4
Heaters, Slat 4	Parting Strip	15.4	1.12	1.12	67.2
	Cycled Zone 1	4.7	2.40	2.40	48
	Cycled Zone 2	5.4	1.28	1.28	25.6
	Cycled Zone 3	5.1	4.39	4.39	87.8

The comparison between TMEDS and ETDS focuses on these aspects of power consumption, de-icing efficiency, mass and cost. Because of time limitation, only the power consumption is calculated above, for the other aspects, a brief discussion is introduced to explain the system advantages and challenges.

The TMEDS and ETDS system architectures are built as mentioned above, and the power consumption requirements for one cycle are obtained. The TMEDS system has a very low consumption, only 0.562 kW. However, conventional ETDS consumes 13.0 kW, which is over 23 times that of a TMEDS. Concerning this comparison, it is clear that TMEDS achieves only a small fuel penalty which makes it a potential ice protection type for power limited aircraft.

TMEDS has high de-icing efficiency, as discussed in Chapter 4.4 and 4.5. Ice accretion is easily removed by the EMEDS with high efficiency due to the weakened interface bond by the PETDS. And the EMEDS is efficient to remove low levels of ice accretion with little energy, so it is feasible to extend the protected surfaces to a larger area which covers the impinged and runback zone, even in SLD conditions, allowing long time flight in icing environment without restrictions. However, for the ETDS, the runback water refreeze is difficult to control and ice formation may occur beyond ice protection area. Therefore, aircraft with ETDS should get out of icing encounters immediately when there is heavy icing intensity. The icing tunnel test of de-icing performance comparison between TMEDS and ETDS is illustrated in Figure 6-3 [1]. It is clear that the downstream ridge is larger in ETDS than that in TMEDS.

TMEDS ETDS

Figure 6-3 Icing Tunnel Tests of TMEDS and ETDS

In contrast with EDTS, TMEDS performs poorer in system mass. The primary components in TMEDS are DCU, ESB, actuators, heaters and cables, whereas EDTS is comprised of WHC, PCU, heaters and cables. For the control units, the DCU and WHC may have almost the same mass, but to the power supply components, An ESB is definitely heavier than a PCU because numerous capacitors are equipped to supply discharging power. Heaters are only limited to the sensitive leading area in TMEDS, less than an ETDS which covers the entire protection surface. However, the heater is usually a very thin metal layer, so the mass difference in heaters can be neglected. The

actuators are distributed along the entire protection area. In addition, in order to install the actuators, a housing with corrugated channels is required in slat structure design. Thus the mass of actuators and support structure may be considerable. Finally, due to having more de-icing zones in an TMEDS, the power cable distribution is more complex than ETDS, which may bring more cable mass in TMEDS. Through the brief discussion above, it can be seen that greater mass of TMEDS may bring a higher fuel penalty than that of ETDS in term of mass. Because of time limitation, the quantified analysis will not be conducted in this project.

As a new technology, TMEDS definitely requires a high cost to reach the engineering application requirements. In order to satisfy the airworthiness certification requirements, a considerable cost will need to be spent on system design analysis, manufacture, and tests. Especially for a new type system, the cost for certification would be much higher. Also the time cost should be considered, because a new technology requires more time in its application on an aircraft. Even if TMEDS gets practical and popular in the aircraft industry in the future, the cost would still be higher than ETDS due to the cost of actuators and capacitors.

The comparison discussed above is summarized in Table 6-6. It is clear that TMEDS has considerable superiority in power consumption and de-icing efficiency, but the system mass is heavier and cost is higher.

Table 6-6 Comparison between TMEDS and ETDS

Items	TMEDS	ETDS
Power	Tiny, 0.562 kW	Considerable, 13.0 kW
De-icing efficiency	Smaller ice ridge: Long time flight in icing condition	Larger ice ridge; Get out of icing encounter
Mass	Heavier	Lighter
Cost	Higher	Lower

Aircraft with certificated ice protection system is able to cope with most icing encounters. However, when the exposure time is too long or icing condition is very heavy, ice will accumulate beyond the system capabilities. So it is advisable for aircraft to exit the icing conditions by changing the flight altitude or path. For a TMEDS, this problem does not exist due to its high de-icing efficiency, allowing flight in icing conditions without restrictions. Thus it can economize considerable fuel which is subject to be burned to change flight route. So the operation cost and fuel penalty are reduced, which offsets its disadvantages over TMEDS in cost and mass. Whether it can overcome these disadvantages, and even turn them into an advantage requires more detailed discussion and calculation.

6.4 Conclusions

In this chapter TMEDS and ETDS system architecture are created based on the civil commercial aircraft Flying Crane in order to compare with each other in terms of system power consumption. During one cycle period, power consumption of TMEDS is 0.562 kW, much less than ETDS with the power level of 13.0 kW. Besides, TMEDS de-icing efficiency is significantly higher to allow long period flight in icing encounters, which may compensate the disadvantages of TMEDS in mass and cost.

7 Summary of the Project

This research project discussed aircraft icing atmosphere and icing effects on aircraft flight performance. Furthermore, the most challenging part, the thermal-mechanical expulsion de-icing technology, was well investigated. The objectives of this study are developed by:

a) Investigating icing meteorology through icing cloud types, meteorological parameters and design conditions.

Two types of clouds are studied, stratiform cloud and cumuliform cloud. Normally, stratiform clouds distribute widely with lower LWC, whereas cumuliform is a vertical type, having higher LWC. In addition, significant icing parameters, such as air temperature, water droplet diameter, liquid water content and exposure time in clouds, have different effects on aircraft icing shape and ice protection system design requirements. For example, critical ice shape is due to high temperature, large droplets, high LWC and large icing extend. The meteorology design conditions and icing detection technology are also introduced briefly.

b) Discussing aircraft icing and icing effects on aircraft.

Three types of ice shapes may accumulate on the surface: glaze ice, rime ice and mixed ice. Glaze ice is denser, harder, and hard to break. It changes the shape of airfoils dramatically and destroys air stream significantly, causing more serious aerodynamic problems. Rime ice typically accretes at a lower rate and forms a more regular shape than glaze ice, and the effects on aerodynamics are not as severe as glaze ice. Mixed ice is a combination of both glaze and rime ice characteristics, and also has harmful effects on aircraft safety.

Aircraft icing causes degraded aerodynamic performance and maneuverability problems due to lift reduction and the drag increases. Ice accumulated on the nacelle may break off and be ingested by engine, which may damage the engine and cause

serious accident. Windshield icing has little effect on aerodynamics performance, but the visibility of the windshield is impaired. In addition, probe icing may result in information indication failure.

c) Introducing various ice protection systems and especially stressing a hybrid system TMEDS, combined with PETDS and EMEDS.

Ice protection system has three categories: thermal, mechanical and fluid. Fluid ice protection system utilizes a fluid to mix with impinged water, lowering the freezing point below the ambient air temperature. Mechanical ice protection systems destroy the cohesion between ice and skin surfaces, and the broken ice pieces are blown away by the air stream. The most striking advantage of such systems is the considerably low power. EMEDS is a novel type of mechanical system, using electromagnetic principles to produce electromagnetic forces to remove ice accumulation with high efficiency. Thermal ice protection system provides heat to the protected surface by hot air or electricity, which has the most common application on aircrafts. In recent years, PETDS has been developed to reduce energy consumption and runback ice accumulation. TMEDS is a hybrid system with the combination of PETDS and EMEDS.

d) Calculating TMEDS power consumption and discussing calculation results.

The calculation of TMEDS power consumption focused on PETDS and EMEDS respectively. The PETDS calculation results indicate that power consumption falls quickly with the increase of pulsing time and considerable power is used to heat the ice and substrate to the melting point. So OAT has significant impact on power consumption. The EMEDS calculation results show that electrical power and electromagnetic force decrease with the increase of turns of coil and rise with the increase of voltage. In addition, the power calculation methods for electro-thermal de-icing are also discussed due to comparison.

e) Building TMEDS system architecture and comparing with ETDS in power

The system architecture is built based on Flying Crane, a civil aircraft. And the power consumption of this TMEDS system is calculated and compared with ETDS. The calculation results indicate that TMEDS has significant superiority in power consumption. Moreover, the contrasts of de-icing efficiency, mass and cost are also discussed briefly. TMEDS has higher cost and heavier mass, while the de-icing efficiency is very high. Due to the high de-icing efficiency, long flight duration in icing conditions is acceptable and may compensate the deficiency in mass and cost.

Therefore, the research objectives of this project are achieved. However, in order to accomplish engineering application, numerous tasks need to be done in the future for TMEDS.

8 Suggestions for Future Work

Because of time limitation, this research only discussed some concepts of TMEDS and calculated system power consumption. Therefore, there are still many tasks needed to be investigated. The suggestions are listed below for further research and development of TMEDS.

a) Aircraft icing calculation and icing effects evaluation should be investigated by aerodynamic methods to determine the ice protection requirements. This job should be done by aircraft icing and aerodynamic researchers.

b) Detailed system parameters calculation, not only system power consumption, but also system mass, volume, cost material properties and so on, should be carried out. In addition, a more accurate calculation method of power consumption should be surveyed, for example, 3-D simulation method can be developed.

c) The calculation mathematical models and system performance should be validated in icing wind tunnel test and natural icing flight test.

References

[1] **Kamel Al-Khalil**. *Thermo-Mechanical Expulsion Deicing System – TMEDS*. AIAA 2007-0692.

[2] **I. Paraschivoiu, F. Saeed**. *Aircraft Icing*. A Wiley-Interscience Publication.

[3] **NASA**. *Stratiform or Stratus Clouds*. [online], 19/07/2010. http://www.grc.nasa.gov/WWW/k-12/Aero2000/studweb/glossary/stratcld.html.

[4] **B. Geerts**. *Stratiform clouds: some examples*. [online], 19/07/2010. http://www-das.uwyo.edu/~geerts/cwx/notes/chap08/stratiform.html.

[5] **G. Fortin, J. Perron, G. Mingione and E. Luliano**. *CIRAAMIL Ice Accretion Code Improvement*. AIAA 2009-3968.

[6] **Federal Aviation Administration**. *Aircraft Ice Protection*. Advisory Circular, AC20-73A, 16th Aug, 2006

[7] **R.J. Hansmann**. *The Influence of Ice Accretion Physics on the Forecasting of Aircraft Icing Conditions*. NASA, Langley Research Center, Joint University Program for Air Transportation Research, 1988-1989, p 63-67

[8] **Ion Paraschivoiu, Octavian Trifu and Farhad Sabri**. *SLD Modeling with CANICE*. [online], 20/07/2010. http://icebox.grc.nasa.gov/documents/cfd-sld-2006/Paraschvoiu.pdf.

[9] **K. Yeoman**. *Efficiency of a Bleed Air Powered Inlet Icing Protective System*. AIAA 94-0717.

[10] **Anil D. Shah, Michael W. Patnoe and Ervin L. Berg**. *Droplet size Distribution and Ice Shapes*. AIAA 1998-0487.

[11] **Kamel Al-Khalil, Richard Hitzigrath**. *Icing Analysis and Test of Business Jet Engine Inlet Duct*. AIAA 2000-1040.

[12] **K. Al-Khalil and E. Irani**. *Tunnel and Natural Icing Tests of a Helicopter Engine Cooling Bay Inlet*. AIAA 2001-0838.

[13] **Héloïse Beaugendre1, François Morency and Wagdi G. Habashi**. *Development of a Second Generation In-Flight Icing Simulation Code*. Journal of Fluids Engineering, Vol. 128, March, 2006, p378-387.

[14] **FAA Technical Center**. *Aircraft Icing Handbook, FAA Technical Report, DOT/FAA/CT-88/8-1,Volume 1*. March, 1991

[15] **Dean R. Miller and Mark G. Potapczuk**. *Preliminary Investigation of Ice Shape Sensitivity to Parameter Variations*. AIAA 2005-0073.

[16] **Deborah A.P. Hersman**. *Aircraft Icing*. Aviation Subcommittee, Committee on Transportation and Infrastructure, February 24, 2010. [onelin], 22/07/2010 http://www.ntsb.gov/speeches/hersman/daph100224.html.

[17] **Wikipedia**. *American Eagle Flight 4184*. [online], 22/07/2010 http://en.wikipedia.org/wiki/American_Eagle_Flight_4184.

[18] **Geoffrey Luxford, David W. Hammond and Paul Ivey**. *Role of Droplet Distortion and Break-up in Large Droplet Aircraft Icing*. AIAA-2004-411.

[19] **S.C. Tan, M. Papadakis**. *Experimental Study of Large Droplet Splashing and Breakup*. AIAA-2007-904.

[20] **Mark G. Potapczuk and Dean Miller**. *Numerical Simulation of Ice Shapes from a Bimodal Large Droplet Icing Cloud*. AIAA- 2006-462.

[21] **M. B .Bragg**. *Aircraft Aerodynamics Effects Due To Large Droplet Ice Accretions*. AIAA-96-0932.

[22] **Sam Lee and Michael B. Bragg**. *Experimental Investigation of Simulated Large-droplet Ice Shapes on Airfoil Aerodynamics*. Journal of Aircraft, Vol.36, No.5, September-October 1999, p844-850.

[23] **Federal Aviation Administration**. *FAR Part 25: Airworthiness Standards: Transport Category Airplanes*. December 16, 2008.

[24] **European Aviation Safety Agency**. *CS-25: Certification Specifications for Large Aeroplanes*. December12, 2005.

[25] **SAE**. AS5498: *Minimum Operational Performance Specification for Inflight Icing Detection Systems*. Society of Automotive Engineers, Inc. October, 2001

[26] **ZHANG Dalin, YANG Xi, ANG Haisong**. *Numerical Simulation of Supercooled Water Droplets Impingement on Icing Surfaces*. Journa of Aerospace Power. Vol. 118 No.11, Feb. 2003

[27] **Civil Aviation Authority**. *Aircraft Icing Handbook*. New Zealand, 2000, Version

1.

[28] **Robert J. Shaw, Mark G. Potapczuk, and Colin S. Bidwell**. *Predictions of Airfoil Aerodynamic Performance Degradation Due to Icing*. National Aeronautics and Space Administration Lewis Research Center, NASA TM-101434, January 16-19, 1989.

[29] **Wikipedia**. *Air France Flight 447*. [online], 06/09/2010. http://en.wikipedia.org/wiki/Air_France_Flight_447

[30] TKS Ice Protection for the Mooney. [online], 08/09/2010 http://www.weepingwings.com/docs/Mooney_No_Hazard.pdf

[31] **FAA Technical Center**. *Aircraft Icing Handbook, FAA Technical Report, DOT/FAA/CT-88/8-1,Volume 2*. March, 1991

[32] **Joseph J. Gerardi, Richard B. Ingram**. *Electro-Magnetic Expulsion De-icing System*. United States Patent, Aug.15, 2000.

[33] **Cox & Company, Inc**. *Low Power Ice Protection Systems*. [online], 10/09/2010 http://www.coxandco.com/aerospace/lowpower_ice_protection.html

[34] **Airbus**. *A319/A320/A321 Aircraft Maintenance Manual*. Feb. 1998.

[35] **Galdemir C. Botura, M.S. Dave Sweet and David Flosdorf**. *Development and Demonstration of Low Power Electrothermal De-icing System*. AIAA-2005-1460

[36] **Galdemir C. Botura, M.S. Dave Sweet**. *Concept Development of Low Power Electrothermal De-icing System*. AIAA-2006-864.

[37] **K. Al-Khalil, T. Ferguson, and D. Phillips**. *A Hybrid Anti-icing Ice Protection System*. AIAA 1997-0302.

[38] **V. F. Petrenko, M. Higa, M. Starostin, and L. Deresh**. *Pulse Electrothermal De-Icing*. Proceedings of the Thirteenth (2003) International Offshore and Polar Engineering Conference Honolulu, Hawaii, USA, May 25–30, 2003.

[39] **Charles Alexander, Matthew Sadiku**. *Fundamentals of Electric Circuits*. Mc Graw Hill Higher Education, 2002.

[40] **R. Elangovan,R. F. Olsen**. *Analysis of Layered Composite Skin Electro-Thermal Anti-Icing System*. AIAA 2008-446.

[41] **B. Rouffie**. Msc Thesis: *Ice Protection System for an All electric Aircraft*.

Cranfield University, Sepetmeber 2003.

[42] **K.J. Dewitt, T.G. Keith, D.F. Chao and K.C. Masiulaniec**. *Numerical Simulation of Electrothermal Deicing Systems*. AIAA-83-0114

[43] **MatWeb**. *The Online Materials Database*. [online], 28/09/2010 http://www.ewp.rpi.edu/hartford/~hawesd/Project/Reference_Material/Material.pdf

[44] **J. Alan, Adams and David F. Rogers**. *Computer-aided heat transfer analysis***.** McGraw-Hill, Inc, 1973.

[45] **S.Thomas, R.Cassoni and C**. *MacArthur. Aircraft Anti-icing and De-icing Techniques and Modeling*. AIAA 1996-0390.

[46] **David W. Hammond & Geoffrey Luxford**. *The Crafield University Icing Wind Tunnel*. AIAA 2003-901

[47] **Cranfield University**. *Main Icing Tunnel*. [online], 08/12/2010 http://www.cranfield.ac.uk/soe/facilities/page11097.html

[48] **AVIC GDP report**. *Flying Crane Desgin Reports*. Cranfield University. 2008~2010.